MARCEL DEKKER, INC. • 270 MADISON AVENUE • NEW YORK, NY 10016

JOURNAL OF DISPERSION SCIENCE AND TECHNOLOGY
Vol. 24, No. 1, pp. 1–41, 2003

FEATURE REVIEW

Dispersion of Carbon Nanotubes in Liquids

Jenny Hilding,[1] Eric A. Grulke,[1,*] Z. George Zhang,[2,*] and Fran Lockwood[2]

[1]Department of Chemical and Materials Engineering and Center for Applied Energy Research, University of Kentucky, Lexington, Kentucky, USA
[2]The Valvoline Company, Lexington, Kentucky, USA

ABSTRACT

Production processes for carbon nanotubes often produce mixtures of solid morphologies that are mechanically entangled or that self-associate into aggregates. Entangled or aggregated nanoparticles often need to be dispersed into fluid suspensions in order to develop materials that have unique mechanical characteristics or transport properties. This paper reviews the effects of milling, ultrasonication, high shear flow, elongational flow, functionalization, and surfactant and dispersant systems on morphology of carbon nanotubes and their interactions in the fluid phase. Multiwalled carbon nanotubes (MWNTs) have been used as an example model system for experimental work because they have been available in engineering-scale quantities and can be dispersed reproducibly in a variety of solvents and polymers. Their size scales, ~30–50 nm in average diameter and ~5–50 microns in length, permit MWNT dispersions to be investigated using transmission electron microscopy, scanning electron microscopy, and in some cases, light microscopy.

Key Words: Carbon nanotubes; Dispersion; Nanotechnology; Milling; Ultrasonication; High shear flow; Elongational flow; Functionalization; Surfactant system; Dispersant system; Morphology.

INTRODUCTION

Multiwalled carbon nanotubes (MWNTs) have an interesting set of properties that position them for a wide variety of potential applications in liquid suspensions, polymer solutions, polymer melts, and polymer composites. Their unusual properties include high moduli of elasticity, high aspect ratios, excellent thermal and electrical conductivities, and magnetic properties. Important challenges to developing applications for these unique materials include: (1) purification and separation of nanotubes by chemistry and morphology; (2) uniform and reproducible dispersion; and (3) orientation of these solids in liquid and melt phases.

*Correspondence: Eric A. Grulke, Department of Chemical and Materials Engineering and Center for Applied Energy Research, University of Kentucky, Lexington, KY 40506, USA; E-mail: egrulke@engr.uky.edu; Z. George Zhang, The Valvoline Company, P.O. Box 14000, Lexington, KY 45012, USA; E-mail: zzhang@ashland.com.

DOI: 10.1081/DIS-120017941
0193-2691 (Print); 1532-2351 (Online)

www.dekker.com

While purification and separation of undesirable byproducts may be needed today, the direction to lower nanotube costs and better product quality lies mainly in learning to control the synthesis chemistry and the reactor system. Work on the catalyst morphology, control of the nanotube growth rate by control of the local environment at the catalyst, and understanding the fouling of the catalyst should lead to reactor systems that provide high quality products at low costs.

The production methods for carbon nanotubes often result in products that have varying diameters and lengths, may be physically or chemically entangled, and may have impurities that should be removed prior to use. Physical entanglement of the nanotubes is defined here as individual particles that are entwined, interwoven, or form loops around other nanoparticles. "Chemical" entanglements can also occur, and can be interpreted as surface-to-surface attraction, adhesion, or self-assembly. For example, single-walled carbon nanotubes (SWNTs) usually associate in bundles, which are thought to minimize the surface energies of the individual tubes. Highly entangled products, that are difficult to disperse uniformly in fluids and melts, result in fluid suspensions and composites with only modest improvements in mechanical or transport properties. Aggregates are generally found to be an impediment to most carbon nanotube applications. The aggregates may not provide three-dimensional networks that efficiently carry mechanical loads or transport properties for the mix or composite, hence losing the desired effects.

There are several methods already demonstrated for control of nanotube orientation once the tubes have been dispersed individually in fluids. These include shear flows, elongational flows, electric fields, and magnetic fields. The preferred orientation for a given application may not mean alignment in one direction: several important applications depend on achieving three dimensional networks of high aspect ratio nanotubes to modify the transport properties of the fluid or solid.

This review article focuses primarily on the second challenge; that of developing reproducible dispersions of carbon nanotubes in liquid phases. Two phenomena affect carbon nanotube dispersions: nanotube morphology and attractive forces between the tubes.

The unique morphology of carbon nanotubes turns dispersion into a challenge. Not only are the tube surfaces attracted to each other by molecular forces, but the extremely high aspect ratios in combination with the high flexibilities dramatically increase the possibilities for entanglements. Entangled aggregates can be difficult to disperse without damaging the nanotubes in different ways. Single-walled carbon nanotubes from research reactors are harvested in bundles, which are very hard to separate into individual nanotubes. Interstitial channels are formed between the tubes in the bundles. These channels may adsorb a larger quantity of gas than the actual nanotube cores do, so for an adsorption type application it might not be of interest to break up the bundles. However, when using SWNTs as a reinforcing agent or conductive filler, dispersing the bundles would increase uniformity and keep production costs down.

Attractive van der Waal's forces between carbon surfaces increase the dispersion difficulty. Carbon surfaces tend to be attracted to each other. For example, studies have shown that dispersion of carbon black in diglycidyl ether-4,4′-diaminodiphenyl sulfone copolymer becomes more difficult as the surface area of the carbon black increases, due to attractive forces between the aggregates.[1] Furthermore, the molecular forces between carbon nanotubes are influenced by both chirality and surface curvature.[2–4] In theory, a highly bent graphite sheet, such as the wall in a carbon nanotube, has strained double-bonds, resulting in a sp^2/sp^3 orbit-hybridization. The double bonds would have partial single bond character and hence the bond would be partially unsaturated. This phenomenon would explain the pronounced attraction between carbon nanotubes. However, recent EELS-experiments show that the curvature has to be extensive to lead to a measurable hybridization,[5–10] thus the effect can be seen for SWNTs, but not for MWNTs.

This review discusses production methods with emphasis on the morphology of their carbon nanotubes products, their typical purity, and methods for removing contamination. Literature references and new data are provided for the effects of milling, ultrasonication, high shear flow, elongational flow, functionalization, and surfactant and dispersant systems on morphology of carbon nanotubes and their interactions in the fluid phase. Processing and dispersion of carbon nanotubes are discussed and new data are presented that indicate a typical rate of nanotube breakage with several of the methods. Carbon nanotube characteristics relating to mechanical strength and transport properties are summarized.

Many of the conventional dispersion methods cause fragmentation (comminution) of the nanotubes, which can be modeled using the moments of the length distribution. As with other solids, the breakage rate of carbon nanotubes depends on their lengths, with the longest particles experiencing the highest breakage rate.

The high aspect ratio of carbon nanotubes can lead to physical contacts between unentangled particles dispersed in fluids, leading to three-dimensional networks that can increase transport properties, such as electrical and thermal conductivity, but can also increase suspension viscosity. The transport property changes can be related to predictions of percolation theory. However,

there are several physical attributes of carbon nanotube suspensions that are not well described by percolation models, including the flexibility of the nanotubes and their orientation under shearing conditions.

SYNTHESIS METHODS AND MORPHOLOGIES

Each production method has a brief description, accompanied by information on the morphologies of the carbon products and their purity. Carbon nanotube purity can be difficult to assess as both residual catalyst and amorphous carbon may be present. Some researchers report purities based on microscopy analyses alone, while others use digestion methods to solubilized non-graphitic carbons and metals. There can be considerable variations in the carbon nanotube morphologies developed using a single synthesis technique.

Vaporization of a Carbon Target

The laser ablation method is based on vaporization of carbon in an inert atmosphere and can produce either SWNTs or MWNTs. The pulsed laser[11–13] evaporates carbon from the graphite target (~1500°C) and the products are transported by an inert gas flow (He or Ar) from the high-temperature zone to a water-cooled copper collector. In the presence of a transition metal catalyst, the method yields between 70 and 90% SWNTs.[12] It has been found that bimetallic catalysts are more efficient.[11,12,14–18] The presence of boron in the system increases the length of the SWNTs, possibly by preventing the closure of the CNT tip and promoting further growth.[19] It has also been noted that, when a porous graphite target is used, the SWNT production is enhanced.[20]

Solar Energy for Vaporization

A solar furnace is used to focus sunlight onto a graphite sample, giving temperatures up to 3000K.[21] The method can be used to produce fullerenes[22–27] in the absence of added catalysts, or either bamboo-shaped MWNTs (Co/Ni, at 250×10^{-3} bar) or SWNTs (Co/Ni at 450×10^{-3} bar, Co or Ni/Y at 7×10^{-8} bar).[26,28–30] The nanotube yield is generally low. Figure 1 shows a typical product.[31]

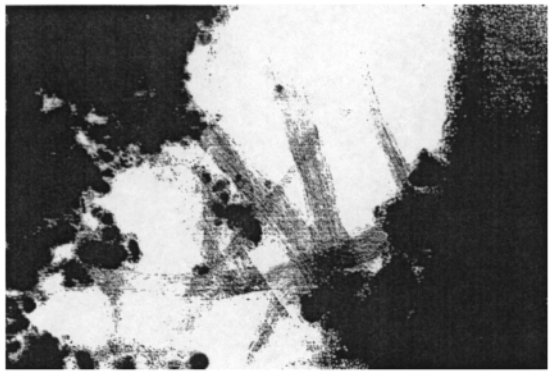

Figure 1. MWNTs generated in a high temperature (3000 K) solar furnace with a graphite target. *Source*: Reprinted from Ref.[31] by courtesy of Elsevier Science.

Electric Arc Discharge

Originally, the electrical arc method was used to produce fullerenes, and MWNTs were found as a by-product.[32] An electric arc is generated between two opposing graphitic electrodes in a reactor filled with He or Ar.[33] A temperature of approximately 4000K is reached between the rods. When one of the electrodes is movable, the reaction is semi-batch. The evaporation of pure graphite[32] produces fullerenes, amorphous carbon, and graphitic sheets on the reactor walls, and fused MWNTs and nanoparticles on the electrode (a typical product is[33,34] $D_i = 1$–3 nm, $D_o = 2$–25 nm, and $L = 1$ μm). The co-evaporation of graphite with a metal or metal salts gives MWNTs on the cathode.[35–42] In some cases, SWNTs can be found as well.[41,43,44] The yield and purity of SWNTs differs depending on the catalyst[45–52] and the presence of H_2 in the reactor.[53] It is possible to produce large quantities of MWNTs per run, but the purity is ~20–50%. Figures 2[54] and 3[55] show typical arc discharge products for MWNTs and SWNTs respectively. The round objects are amorphous carbon and residual metal catalyst.

Electrolysis

Electrolysis using a graphite rod cathode and a molten lithium chloride anode can be used to produce a wide range of nanomaterials. The process takes place in a furnace either in air or under inert conditions. A current (3–5 A for nanotube production) is applied through the graphite rod, the cathode erodes and particles can be found dispersed in the melt after 3–4 min.[56,57] The solid product is extracted into a toluene phase. Spiral and

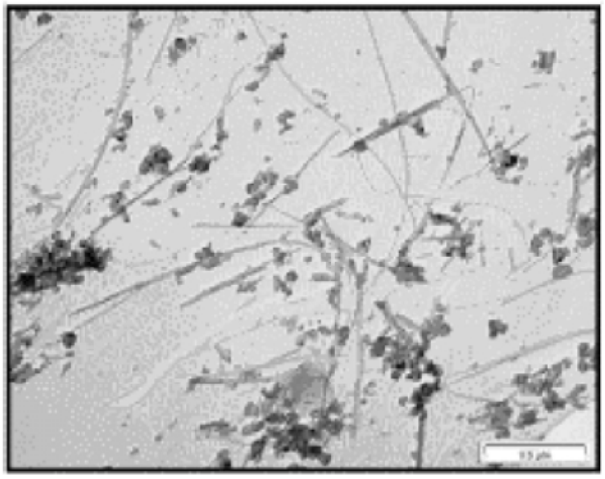

Figure 2. Electric arc discharge MWNT product. *Source*: Reprinted from Ref.[54] by courtesy of Elsevier Science.

curled CNTs are produced with $L \leq 5\,\mu m$ and $D_o = 2$–$20\,nm$.

Chemical Vapor Deposition

Chemical vapor deposition synthesis depends on metal catalysts that can be deposited on a substrate, either in situ or prior to nanotube synthesis. Nanotubes grow as a gaseous carbon source, usually a hydrocarbon, decomposes on the catalyst particles and forms graphitic carbons. Temperatures range from 873 to 1273°C in most systems. The produced MWNTs have high purity and are relatively long, with lengths reported even on the millimeter-scale.[58] A wide range of metals have been investigated as catalysts.[59–68] The morphology of the tubes varies with the chosen catalyst[60,61,66,69] and by using a feed-gas containing nitrogen,[61,70] it is possible to incorporate significant amounts of nitrogen in the tubes. CVD has also been used to produce SWNTs.[71–73] Bimetallic catalysts are predominantly used to produce SWNTs, but can catalyze the growth of MWNTs as well. Figure 4 shows a typical MWNT product from the CVD synthesis based on ferrocene as the metal precursor and xylene as the carbon source[59]. The tube-sides and ends are shown closer in Fig. 5. Mechanical removal of the MWNTs from the reactor sufaces fractures the nanotubes. There are distributions of diameters and lengths throughouth the reactor, and typical aspect ratio varies from 500 to 2000. At a specific location in the reactor, the nanotubes are of uniform lengths.

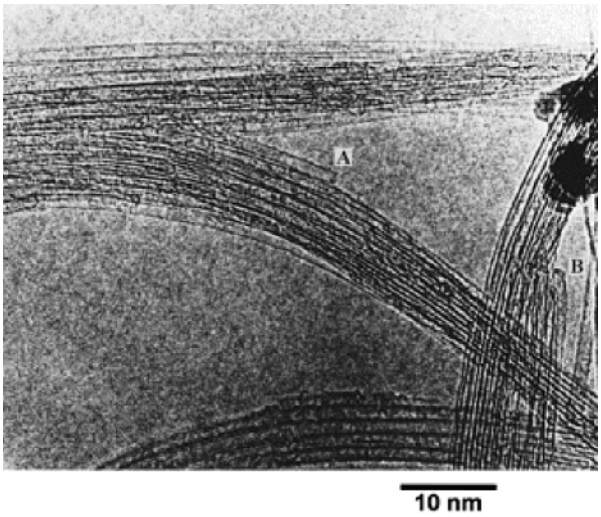

Figure 3. Electric arc discharge SWNT product. *Source*: Reprinted from Ref.[55] by courtesy of Elsevier Science.

Sonochemical Production of Carbon Nanotubes

Nanotubes can be produced through a homogeneous sonochemistry process.[74] The reaction is very fast and takes place at the "hot spot" created right at the tip of the sonication probe, where the temperature is thought to reach over 5000K. The molecules in the hot spot get pyrolyzed; with a liquid–solid mix (e.g., benzene–metal particles), the reaction takes place on the liquid–solid interface. However, the organic liquid can decompose and/or form polymers. *o*-Dichlorobenzene in combination with $ZnCl_2$ produces highly crystalline nanotubes. Figure 6 shows a typical product,[74] having an aspect ratio of 40.

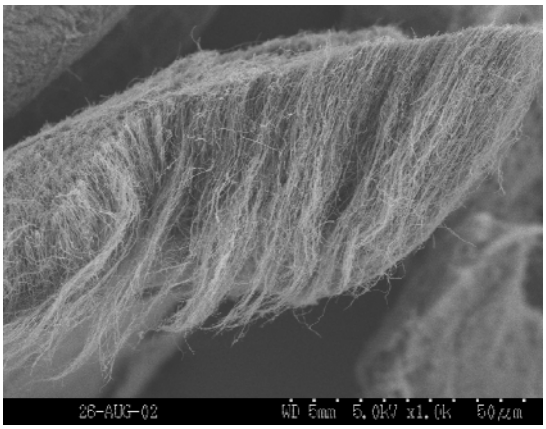

Figure 4. MWNTs from CVD synthesis based on ferrocene and xylene at 1023 K.

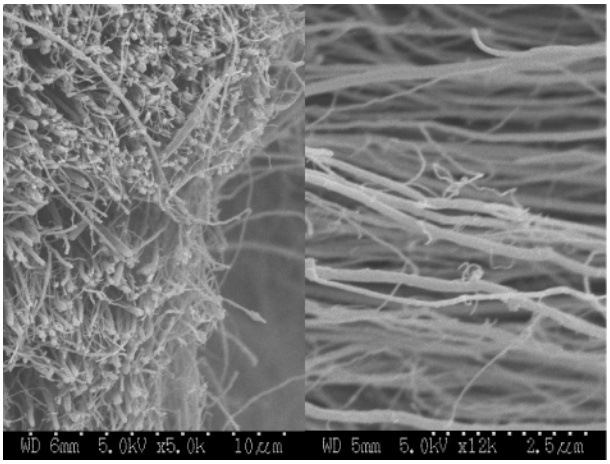

Figure 5. Close-up of CVD synthesized MWNTs, showing ends and side-walls.

Low Temperature Solid Pyrolysis

This method is used to produce capped MWNTs *in situ*,[75] with a morphology of $L = 0.1$–$1\ \mu m$, $D_i \geq 1.02$ nm, and $D_o = 10$–25 nm. A refractory metastable compound, such as nano-sized silicon carbonitride, is used as the carbon source. The powder is pyrolyzed for 1 hour in an N_2-filled graphite furnace at temperatures between 1500–2200°C ($T_{optimum} = 1700$°C). The tubes are formed on the powder surface and SCN is found in the hollow core. Figure 7 shows a typical product[75] with an aspect ratio of 28.

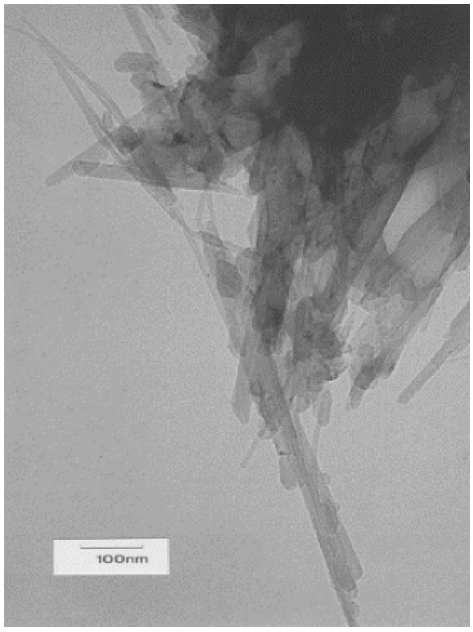

Figure 6. Sonochemical production of nanotubes. *Source*: Reprinted from Ref.[74] by courtesy of Elsevier Science.

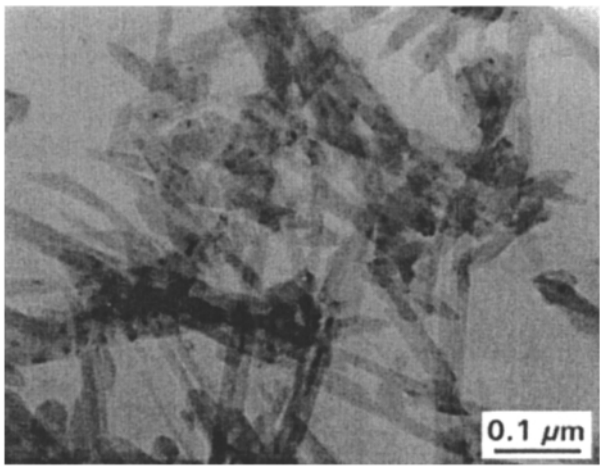

Figure 7. Solid pyrolysis of silicon carbonitride at 1673 K. *Source*: Reprinted from Ref.[75] by courtesy of Materials Research Society.

Catalyst Arrays

A porous anodic aluminum oxide template (thickness of 1 μm, hole diameter of 80 nm) was used to create MWNTs of uniform length and diameter.[76] The produced nanotubes have uniform thickness, but uneven lengths, compared to the CVD produced MWNTs as seen in Fig. 8. The nanotube products could be cut by sonicating the template. After the production is complete the template is etched away, leaving nanotubes of even morphology and good crystallinity.

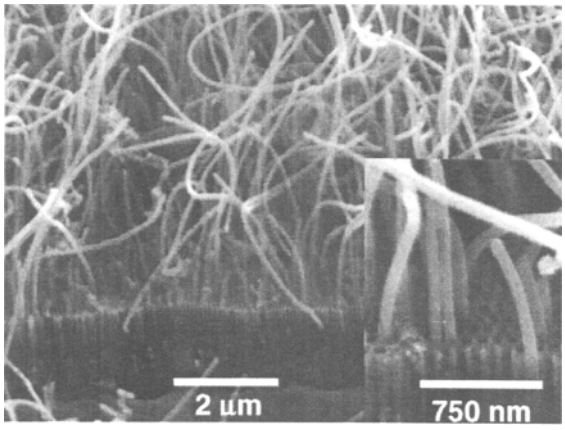

Figure 8. Production of nanotubes by catalyst arrays. *Source*: Reprinted from Ref.[76]. Copyright (2002) American Chemical Society.

Single-walled carbon nanotubes and MWNTs are produced in situ by reducing a composite metal oxide powder in a H_2–HC atmosphere.[77] A nanotube net is created consisting of both SWNT bundles ($D_{bundle} <$ 100 nm, L_{bundle} up to 100 μm) and MWNTs ($D =$ 1.5–15 nm). An example of a typical product can be seen in Fig. 9. Figure 9(a) and (b) show SWNTs partially separated from bundles and Figure 9(c) shows the layered annuli of MWNTs.

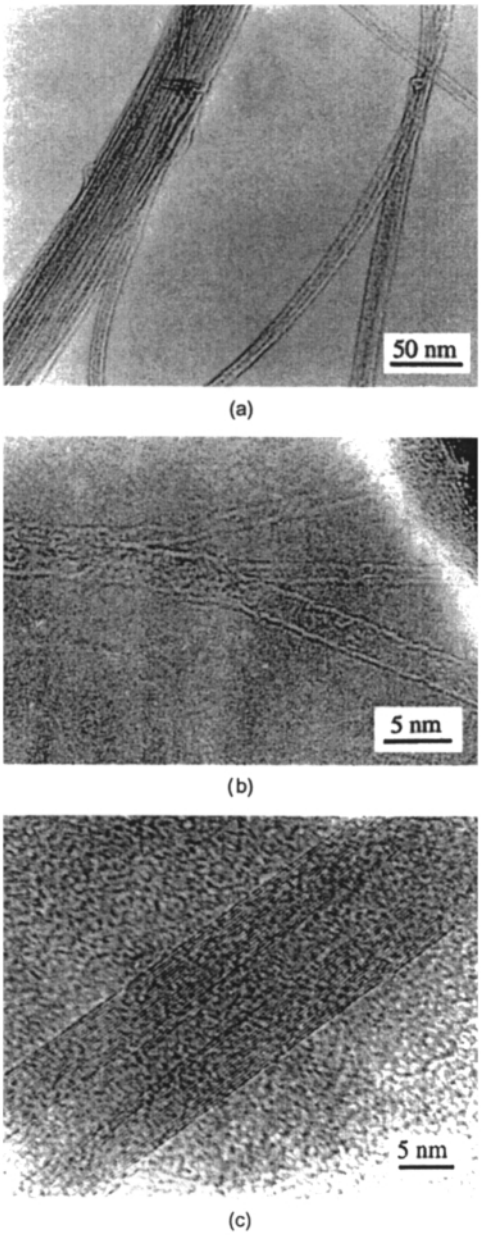

Figure 9. In-situ production of carbon nanotubes. *Source*: Reprinted from Ref.[77] by courtesy of Materials Research Society and Dr. A. Peigney.

Synthesis from Polymers

Carbon nanotubes can be synthesized from the carbonization of emulsion copolymers of polyacrylonitrile (PAN) and poly(methyl methacrylate) (PMMA). Microspheres with an outer shell of PAN and a center of PMMA are blended with a PMMA matrix and spun into fibers. Heat-treatment for 30 min at 900°C in inert atmosphere results in complete consumption of PMMA and carbonization of PAN to MWNTs.[78] The microsphere sizes determine the size of the nanotubes produced and the PAN-shell thickness determines the nanotube wall-thickness. In another process a polymer primarily consisting of carbon is chemically treated to promote polymerization.[79] The treatment is followed by a 400°C heating session in an air filled furnace for 8 hrs. The product consists of MWNTs with $D = 1$–20 nm and $L < 1$ μm. Figure 10 shows a typical product.

Summary of Nanotube Morphologies

Figures 1–10 illustrate the wide range nanotube morphologies available from the various synthesis methods. There are differences in purity, yield, aspect ratio, nanotube diameters, surface structures, defects, densities,

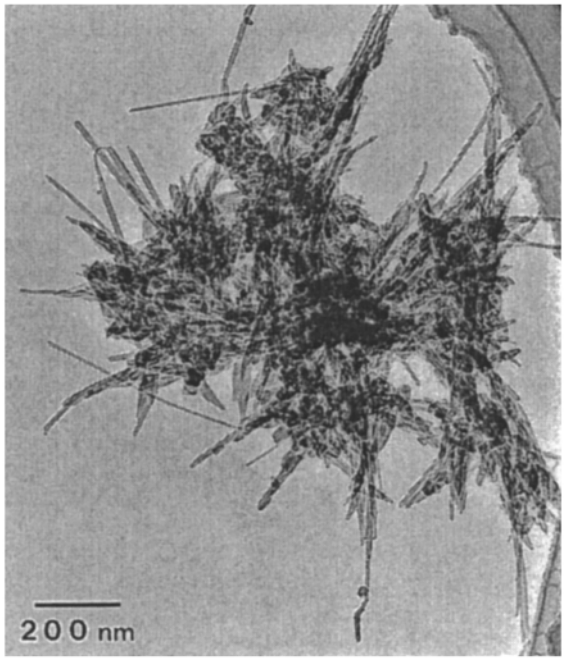

Figure 10. Production of carbon nanotubes from bulk polymer. *Source*: Reprinted from Ref.[79] by courtesy of American Institute of Physics.

and physical entanglements. The nanotube characteristics can be manipulated by changing processing and reactor conditions. Only in a few circumstances is the reactor product of desired morphology for the application. High temperature processes, such as laser vaporization and the electric arc, can have wide temperature ranges in the reaction zone. CVD and catalytic array processes require that the nanotubes be mechanically removed from surfaces. Electrolysis, sonochemical, and low temperature solid pyrolysis require that the products be removed from liquid phases. A long-term scientific objective is to be able to fabricate nanotubes to specific diameters and lengths at precise locations, however, these types of experiments are not yet carefully investigated. Therefore, it is important to be able to disperse the reactor product as uniformly as possible for further processing, which is the focal point of this article.

CARBON NANOTUBE PROPERTIES

Carbon nanotubes are examples of nanoparticles with very high aspect ratios, high mechanical properties, and intriguing transport properties. As such, they constitute a useful model system for evaluating the potential of nanoparticle additives to liquids and polymeric solids for achieving significant improvements in bulk properties at low volume loadings.

While there are many unusual properties of carbon nanotubes, the focus in this section is mechanical and transport properties because of their potential engineering and product applications. Tensile, compressive and flexural moduli should relate to carbon nanotube performance in structural composites. Electrical and thermal conductivities are important in developing conducting suspensions and polymeric solids. Changes in these transport properties when the nanotube is under mechanical strain, could be important for electrical and nanomechanical devices.

It is tempting to apply the rule of mixtures to estimate the properties of carbon nanotube suspensions and composites. As with other filled systems, this rubric is only a first approximation and could very well provide a poor estimate since dispersion, orientation, and the interphase linking the nanotubes to the continuous phase all affect the bulk properties of the material. Percolation theory may apply to transport properties of suspensions and composites, but also may have significant limitations. Despite our limitations in predicting suspension and composite properties, the physical property data of this section can be used to compare carbon nanotubes to other potential additives, to develop estimates of mixture properties, and to illustrate the potential variation in physical properties of these materials.

Computed and Measured Properties of Single-Walled Carbon Nanotubes

Single-walled carbon nanotubes properties can be modeled using molecular dynamics simulations, and there are many predictions on their physical properties. Measuring these properties can be difficult, as it is difficult to isolate single SWNTs for study. The unusual properties of carbon nanotubes could lead to many bulk and surface applications. Some estimates give thermal conductivity of carbon nanotubes two times larger than that of a diamond and they are thermally stable up to 2800°C in vacuum. The electrical carrying capacity is a thousand times larger than that of copper wires.[80] If SWNTs are pressurized up to 55 GPa, the tubes do not collapse, but a superhard phase can be created (SPSWNT) having a hardness in the range of 62–150 GPa.[81] Single-walled carbon nanotubes have different helicity, depending on to what angle the graphene sheet is rolled up. The helical structure is denoted by two integers, (m, n), that indicate the number of lattice vectors in the graphite plane.[82] For chiral structures, the integers are $(2n, n)$; for zig-zag, $(n, 0)$; and for armchair, (n, n). The physical properties of the tube, especially the electrical properties, are dependent on the helicity.

Molecular dynamics studies show that axial deformation of SWNTs at 0 K is strongly dependent on helicity. Armchair and zig-zag are the stiffest structures.[83] Armchair and chiral are of metallic character, while zig-zag is semi-conducting.

Bending the tubes changes their electrical properties. Topological defects increase the electrical resistance of metallic NTs. For the metallic chiral tube, bending introduces a metal-semiconductor transition manifesting itself in the occurrence of effective barriers for transmission. Zig-zag nanotubes remain semi-conducting ($d < 1.5$ nm) and the armchair configuration keeps the metallic character during bending ($d > 0.7$ nm).[84]

Bending and twisting a MWNT changes its electronic transport properties. No effects were seen for low strains, but when high strains were applied, the MWNT morphology changed resulting in drastic effects in the local electron structure of the tube.[85] It has also been seen that the transmission function decreases for twist >4°. When the tube is twisted, the electrical resistance increases, especially for angles larger than 45°. This is strain enough to result in kinks, introducing α–π hybridization.[86] Also, for strains greater than 5% (at high

temperature), pentagon–heptagon defects are spontaneously formed, since they are energetically favorable. This can lead to an onset of plastic deformation of the nanotube (Hooke's law or Stone-Wales transformation).[87] This type of configuration deformation can be seen as a singularity in the stress-strain curve, due to energy release.

Mechanical Properties

Multiwalled carbon nanotubes consist of one or more seamlessly rolled up graphene sheets, with typical shell separations of 0.34 nm.[88] In the absence of mechanical entanglements, MWNTs tend to exist as individual particles in suspensions with many organic liquids. Carbon nanotubes are extremely strong, 30–100 times stronger than steel, but with only one-sixth of its weight.

Table 1 shows measured values of the mechanical properties of MWNTs. The measured values of their Young's moduli are in the range of 10^3 GPa. Tensile strengths may be in the range of 50 GPa, with compressive strengths perhaps a factor of two larger. Individual tubes are susceptible to bending, and can recover their original shape after deformation.

Table 1. Mechanical properties of MWNTs.

Properties	Value (GPa)	Reference
Measured		
Outer shell strength	11–63	[89]
Young's modulus	810 ± 410	[90]
Young's modulus	450	[91]
Young's modulus	1.8×10^3	[92]
Young's modulus	1.3×10^3	[93]
Young's modulus	270–950	[89]
Elastic modulus	$1.28 \pm 0.59 \times 10^3$	[93]
Young's modulus, radial compression	9.7–80.8	[94]
Tensile strength	~10–60	[89]
Tensile strength	3.6	[91]
Axial elasticity	~200–400	[89]
Compressive strength	~100	[89]
Compressive strength	5.3	[94]
Bending modulus, MWNTs with bamboo-type structure	23–32	[95]
$D < 8$ nm	1.2×10^3	
$D > 30$ nm	0.2×10^3	
Average bending strength	14.2	[93]
Average bending strength	~14	[89]
Average bending strength	14.2 ± 8.0	[95]
Calculated		
Young's modulus	1.0×10^3	[88]

Mechanical properties can be measured in a few different ways. The tip of an atomic force microscope (AFM) can be used to measure the mechanical properties of carbon nanotubes in many ways. One way is to place the tube over an alumina ultrafiltration membrane and push on the side of the tube with the AFM tip. The deflection is recorded as a function of the force.[90,96] This type of experiment has also been carried out using a scanning probe microscope (SPM) tip.[94] If a carbon nanotube is mounted between two opposing AFM tips, the outer shell strength can be measured when the tube is pulled apart.[89] One experiment has even been done with a specially designed stress–strain puller to measure Young's modulus of thin ropes consisting of aligned MWNTs.[91] The tubes can also be attached between a surface and an AFM tip and pulled.[97] TEM can be used to measure the intrinsic thermal vibrations of tubes. From these measurements, the modulus can be calculated.[92,98] An oscillating voltage of the right amplitude applied on the nanotube can also induce a mechanical resonance.[95] One of the carbon nanotube ends can also be pinned to a surface and pushed from the side.[93]

Measurements of the elastic modulus (Young's modulus) are usually done by atomic force microscopy,[93] and give results in the range of 10^3 GPa, giving reasonable agreement with theoretical estimates.[88] The radial compression shows an interesting nonlinearity with the applied stress, resulting in an elastic modulus that increases with compression.[94] Compressive strengths depend on the MWNT morphology, since the failure mode in compression is the bending of the tubes.[95] Most high strength fibers are brittle, but carbon nanotubes can have very large strains at their yield point, perhaps as much as 0.30.

Single-walled carbon nanotubes are more flexible than MWNTs and generally self-assemble into bundles as a way to minimize surface energy. These bundles can be very difficult to disperse. The mechanical properties of SWNTs are more difficult to measure due to their small size. Furthermore, since the SWNTs are usually arranged in ropes, it is hard to measure the physical properties for one single tube. Table 2 gives some measured and calculated properties of SWNTs and SWNT bundles or ropes. Surprisingly, some measured values for the Young's moduli of SWNT ropes are similar to the calculated values of single SWNTs. Also, the bending moduli of SWNTs with different helicities are quite similar.

Table 3 provides mechanical properties of several other carbon-related materials with high and low aspect ratios. Diamond exists as a three-dimensional structure of

Table 2. Mechanical properties of SWNTs.

Property	Value (GPa)	Reference
Measured		
Young's modulus	1.25×10^3	[98]
Young's modulus, SWNT ropes	320–1470	[97]
Young's modulus, SWNT ropes	6.5 ± 4.10	[96]
Tensile load	13–1470	[97]
Average bending strength	14.2 ± 8	[96]
Shear modulus	6.5 ± 4.10	[96]
Calculated		
Young's modulus	764	[99]
Young's modulus	1×10^3	[100]
Young's modulus	674	[101]
Armchair	641	
Zig-zag	648	
Young's modulus	0.97×10^3	[102]
Young's modulus		[103]
Variation with radius	0.95×10^3–1.2×10^3	
Variation with helix angle	1.02×10^3–1.08×10^3	
Young's modulus	320–1470	[97]
Young's modulus	1.22×10^3	[104]
Tensile strength	6.249	[99]
Breaking strength	13–52	[97]
Bending modulus		[101]
armchair	963	
Zig-zag	912	
chiral	935	
Bending modulus		[104]
(10,0), (6,6)	1.22×10^3	
(10,10)	1.24×10^3	
(10,5), (15,15)	1.25×10^3	
(20,0)	1.26×10^3	

carbon with sp^3 bonds. It is the hardest material known (hardness = 109,000 kg/mm^2), and has excellent tensile (3.5 GPa) and compressive strength (110 GPa). Graphite has low mechanical strength and is often used as a low friction coefficient material since the graphitic planes can easily slip past each other. Carbon nanotubes, graphite and diamond have similar Young's moduli. Generally, all are stronger than vapor-grown fibers.

Transport Properties of Carbon Nanotubes

The transport properties of carbon nanotubes are high compared to many solids; see Table 4. Percolation theory suggests that highly conductive, high aspect ratio solids could produce three-dimensional networks with high transport properties. The thermal and electrical conductivities of single nanotubes are thought to be higher than graphite, although the more important number may be the conductivity of three-dimensional networks of these solids. For example, defect densities may have a larger effect on transport properties than on mechanical properties.

The transport properties of graphite and diamond are shown at the end of Table 4 for comparison. The thermal conductivity of diamond is one of the largest known (2000 W/m K). The thermal conductivity of graphite along its planar direction is also very high (1000 W/m K) while the value perpendicular to the plane is fairly low. Measurements and computations for the thermal conductivity of an individual single wall nanotube exceed those for diamond. However, when the computations are performed for bundles of SWNTs, the expected morphology in most systems, the values resemble those of in-plane and cross-plane graphite. Measured and computed values for the thermal conductivities of MWNTs are also similar to those of graphite. At least one measurement is several orders of magnitude lower, suggesting that defects in the MWNTs significantly affect their transport properties. The electrical resistance of MWNTs appears to be higher than that of SWNTs, and similar to the values for graphite. Diamond is an excellent thermal conductor but acts like a semiconductor in terms of electronic properties.

Transport Properties of Nanotubes Dispersions and Composites

Electrical Properties

The electrical properties of a composite are measured in terms of resistance. Well-dispersed electrical fillers create a three-dimensional network, which provides a conductive path through the composite. This is a commercial way to turn an insulating material into an electrical conductor. The loading limit is called the percolation threshold and can be detected as a sharp drop in electrical resistance. Single-walled carbon nanotubes in epoxy have percolation limits of 0.1–0.2 wt.% or 0.04 vol%,[126,127] while it has been determined that the percolation limit for nanotubes in PMPV is as high as 8.5 wt.%.[128] Figure 11 shows the change in electrical conductivity of an MWNT-filled epoxy as a function of nanotube volume fraction. The nanotubes were mixed into the epoxy and had an average aspect ratio of 323. At a MWNT loading of about 1 wt.%, there is a large reduction in the material's electrical resistance. Low levels of carbon nanotubes could result in large increases in the thermal and electrical conductivities of liquid suspensions and polymer composites. For comparison,

Table 3. Mechanical properties of high and low aspect ratio solids.

Material	Property	Result (GPa)	Reference
Measured			
Carbon fibers	Young's modulus	900	[105]
Carbon fibers	Elastic modulus	100–800	[106]
Carbon fibers		695	[107]
Graphite	Young's modulus	1.06×10^3	[108]
Graphite (Compression-Annealed Pyrolytic Graphite)	Young's modulus	1.02×10^3	[109]
SiC-nanorods	Bending strength	53.4	[95]
SiC nanowires	Young's modulus	20–32	[95]
SiC–SiO nanowire (SiC in wire core, SiO in sheath)	Young's modulus	46–81	[95]
Calculated			
SiC–SiO nanowire (SiC in wire core, SiO in sheath)	Young's modulus	73–109	[95]
Graphite	Young's modulus	0.97×10^3	[102]
Graphite	Young's modulus	1060	[110]
Graphite	Young's modulus	1.02×10^3	[111]
Vapor-grown fibers	Young's modulus	0.15×10^3	[112]
Diamond	Young's modulus	1.2×10^3	[113]
Vapor-grown fibers	Tensile strength	2.6	[114]
Graphite	Tensile strength	20	[114]

some typical percolation threshold limits for other fillers are 9–18 wt.% for vapor-grown carbon fibers in polypropylene,[129] 15 wt.% for Cu-powder,[130] 35 wt% for Al-powder,[131] and 20–40 wt.% in epoxy for carbon black.[127,131] Such high concentrations will most likely compromise the physical properties of the matrix and do not result in multifunctional materials. The positive conductive effect of carbon nanotube filler is dramatic. It has been reported that the electrical conductivity of PPV increases eight times by introduction of SWNTs in the matrix.[132] Adding MWNT to PMPV increases the electrical currency from 2×10^{-10} S/m to 3 S/m.[128] The electric conductivity increased by 340% for fiber spun from petroleum pitch containing 5 wt.% purified SWNTs.[133] As little as 0.1 vol% nanotubes increases the matrix conductivity of the electrical insulator epoxy to 1 mS/m.[127] Metal oxides can also be converted from insulators to conductors by hot-pressing the MeO powder, an insulating material, with nanotubes at moderate temperatures (1200°C), resulting in an electrical conductivity between 0.2–4.0 S/cm.[134] To avoid electrical charging of an insulation material, a matrix conductivity of 1 μS/m is necessary. At hot-pressing temperatures above 1500°C, the nanotubes get destroyed and the composites turn into insulators again.

As mentioned previously, the nanotube alignment in the matrix is of importance and can improve the electrical properties even further. It has been observed that the electrical conductivity is higher in the flow direction than perpendicular to the flow-direction (0.1–12 vs. 0.08–7 S/m) for solvent cast and hot-press melt-mixed PMMA with SWNTs.[135] It is also worth noting that when SWNTs are ground prior to film-casting, the emission current is improved. Films made with ground tubes show more free nanotube ends sticking out perpendicular to the surface, which might be an explanation for this effect.[136]

Mechanical Properties

Another way to determine whether the carbon nanotubes are well dispersed in a matrix is to investigate the mechanical properties of the composite. If the mechanical properties increase, the dispersion is most likely uniform throughout the matrix. If the dispersion is poor, the mechanical properties will decrease relative to the pure polymer matrix.

The Vicker's hardness is 3.5 times higher for epoxy with a SWNT loading of 2 wt.%, compared to pure epoxy. This result indicates good dispersion.[126] When loading the epoxy with 5 wt.% MWNT, the tensile strength increases from 3.1 GPa to 3.7 GPa and the compressive modulus increases from 3.6 GPa to

Table 4. Transport properties of carbon nanotubes, graphite, and diamond.

Properties	Value	Unit	Reference
SWNT			
Thermal conductivity	6000	W/m K	[115, 116]
Thermal conductivity[a]	2400–2900	W/m K	[117]
Thermal conductivity, axial, bundles[a]	950	W/m K	[117]
Thermal conductivity, radial, bundles[a]	5.6	W/m K	[117]
Critical burn-out current	10^9	A/cm^2	[118]
Electrical resistance		kΩ	[119]
Fiber spun from 200 SWNTs	0.065		
Fiber spun from 100 SWNTs	10		
MWNT			
Thermal conductivity (300K)	900	W/m K	[120]
Thermal conductivity (300K)[a]	1980	W/m K	[121]
Thermal conductivity, high defect ratio, (300K)	25	W/m K	[91]
Current density	1×10^3	A/cm^2	[122]
Critical burn-out current	$100–600 \times 10^{-6}$	A	[122]
Critical burn-out current	200×10^{-3}	A	[123]
Specific heat, 300K	~0.430	kJ/kg K	[91]
Electrical conductivity	1000–2000	S/cm	[122]
Electrical resistance	6–120	kΩ	[123]
Electrical resistance ($T = 10–300$)	2.0–3.5	kΩ	[91]
Graphite			
Thermal conductivity, *x*-plane[a]	1000	W/m K	[117]
Thermal conductivity, *y*-plane[a]	5.5	W/m K	[117]
Electrical resistance, in-plane	1.7×10^{-6}	Ω cm	[124]
Electrical resistance, perpendicular to in-plane	3.7×10^{-3}	Ω cm	[124]
Diamond			
Thermal conductivity	2000	W/m K	[125]
Electrical resistivity	10^{13}	W cm	[125]

[a]Theoretical values.

4.5 GPa.[137] Introduction of 1 wt.% MWNT in a polystyrene matrix increases the elastic modulus by 36–42% (to 450 MPa) and the break stress by 25%.[138] There are quite a few reports on nanotube-fillers in PMMA. The effects of fairly low amounts of nanotubes in PMMA are generally positive, as only 1 wt.% NT in PMMA increased the elastic modulus by 30%.[139] One method developed to incorporate MWNTs in PMMA is to use the free radical-initiator AIBN (2,2-azobisisobutyronitrile) to polymerize the PMMA. When as-grown tubes (1–3 wt.%) are used as a filler, an increase in toughness, tensile strength, and hardness is observed. If the MWNTs used are purified (98% pure), toughness, tensile strength and hardness increase 34%, 31%, and 48%, respectively, for a loading of 1–10 wt.%. If the MWNT loading exceeds 20 wt.%, the tubes are not completely wrapped in the polymer and the positive effects are lost.[140]

Another mixing method is melt-blending MWNTs in PMMA at low temperatures (200°C). The storage modulus increases, especially at high temperatures. It has been observed that by adding 30 wt.% MWNTs, the storage modulus is increased by a factor of 1.4 at 40°C and a factor of 6.0 at 120°C.[141] Furthermore, adding a small amount of poly(vinylidene fluoride) (PVDF) increases the storage modulus dramatically. For example, adding 0.5 wt.% PVDF to the matrix doubles the storage modulus compared to a pure MWNT/PMMA composite. The improvement is temperature-dependent, since the glass transition temperature, T_g, decreases for the mix when PVDF has a lower T_g than PMMA. The lower T_g means that the composite gets softer, or has a lower storage modulus, at higher temperatures. The percentage of PVDF has to be kept low in the composite, so as not to weaken the matrix.[142] The mechanical improvements on

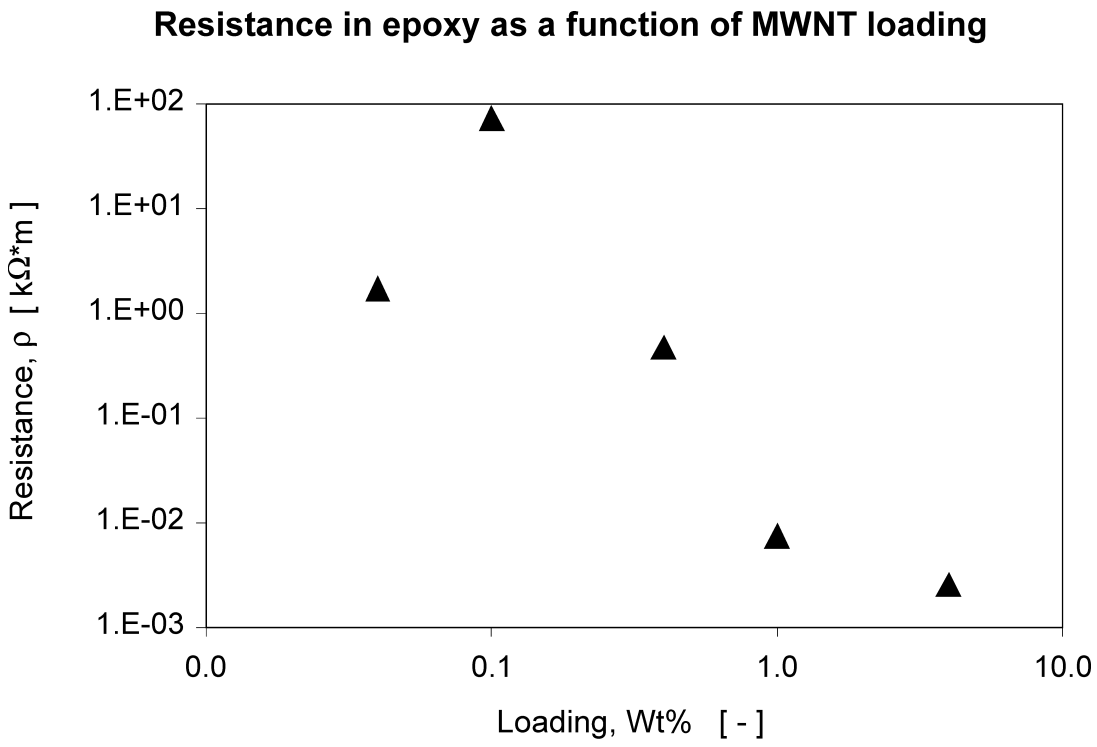

Figure 11. Electrical resistance of an MWNT-filled epoxy as a function of nanotube volume fraction.

adding nanotubes to an amorphous polymer, as opposed to a semi-crystalline polymer, can be greater since the semi-crystalline polymer is already stiff.

The mechanical properties of fibers produced with carbon nanotubes have been investigated as well. When 5 wt.% purified SWNTs were spun with isotropic petroleum pitch, the tensile strength increased by 90% (from 500 to 800 GPa) and the elastic modulus increased by 150% (from 34 to 78 GPa).[133] Nanotube ribbons and fibers have also been produced by recondensing SWNT-surfactant dispersions in a poly(vinyl alcohol) solution. The elastic modulus was measured at 9–15 GPa, which is 10 times higher than the modulus of high-quality bucky paper.[143] The fibers contain aligned SWNT bundles and can be tied into a tight knot.[144,145]

Finally, carbon nanotubes have also been used to reinforce metallic compounds, with various results. The dominating blending method in these cases is hot-pressing at temperatures around 1200–1300°C. It has been reported that when nanotubes are hot-pressed with metal oxides, the fracture strength and toughness decrease with loading,[134] while when hot-pressed with nanophase alumina powder, the fracture toughness increases from 3.4 to 4.2 $MPa/m^{1/2}$[146] for a loading as high as 10 wt.%.

Thermal Properties

It is also possible to improve the thermal stability of a composite by adding carbon nanotubes. It has been shown that by adding 1 wt.% SWNTs to an epoxy matrix, the thermal conductivity increases 120% to 0.5 W/m K at room temperature and 40% at 40K. The thermal conductivity increases 60% for a 0.5 wt.% SWNT load at room temperature.[126] By adding 1 wt.% nanotubes in PMMA, the glass-transition temperature, T_g, increases from 66 to 88°C[139] and the heat-deflection temperature increases as well.[140] The degradation temperature increases with 30°C for a MWNT loading of 26 wt.%.[141]

Clearly, the transport properties of nanotube suspensions and composites can be altered by the addition of carbon nanotubes. Control of the dispersion methods is important to developing uniform and reproducible properties in these applications.

DISPERSION METHODS

As shown in the first section, a number of the current synthesis methods produce nanotubes that are physically

entangled. One objective of dispersion science and technology is to produce a suspension of independent, separated nanotubes that then can be manipulated into preferred orientations in one-dimensional (fiber), two-dimensional (flat sheet), or three-dimensional (bulk solid) objects. There are two different approaches to nanotube dispersion: mechanical (or physical) methods and chemical methods. Mechanical dispersion methods, such as ultrasonication, separate nanotubes from each other, but can also fragment the nanotubes, decreasing their aspect ratio during processing. Chemical methods use surfactants or functionalization to change the surface energy of the nanotubes, improving their wetting or adhesion characteristics and reducing their tendency to agglomerate in the continuous phase solvent. However, aggressive chemical functionalization, such as using neat acids at high temperatures, can digest the nanotubes. Both mechanical and chemical methods can alter the aspect ratio distribution of the nanotubes, resulting in changes in the properties of their dispersions.

Measurement and Analysis of Nanotube Length Distributions

Many mathematical functions have been used to model the particle size distributions of comminution processes. These functions include empirical models as well as probability density functions. As particles are fragmented and broken during processing, their length distributions change as do the model coefficients that describe the distributions. Probability density functions are particularly useful if they provide a good fit to particle size distributions since the moments of the distributions can be used in kinetic rate models that predict the change in the length distributions with time. These kinetic rate models have been used to interpret the reduction of chain lengths during processes such as catalytic or thermally induced polymer degradation and polymer ultrasonication. Gel permeation chromatography of polymers yields complete differential distributions that provide rich information on the fragmentation process. A key assumption of these models is that one fragmentation event occurs in the chain (or particle or nanotube) at a time, an assumption that would be met by most mechanical processes of nanotubes.

Typical Particle Fragmentation Distributions

The rates of particle fragmentation for most minerals, ceramics, metals, and polymers generally decrease as the characteristic particle size decreases. As the materials fragment to smaller sizes, less of the applied energy results in fragmentation and more is lost through particle motion, particle compression, particle flexing, and other mechanisms. A simple kinetic rate model based on binary fragmentation that can describe these phenomena is:[147–149]

$$-\frac{dL}{dt} = kL^b \tag{1}$$

where L is a characteristic material length, t is time, k is a rate constant, and b is the exponent that describes the change in fragmentation rate with length. When $b = 1$, Eq. (1) describes a first order comminution process that does not depend on chain length. We anticipate that nanotube fragmentation will depend on length. The previous references demonstrate how continuous distributions can be analyzed to determine the coefficients, k and b, and the new product distributions at any time, t. This elegant approach is beyond the scope of this article as it assumes that each nanotube will be exposed to similar processing conditions of energy per unit volume, simple shear, elongational flow or mechanical force. Except for suspensions with low concentrations of nanotubes, these conditions may not be met for many of the methods. Some of the practical problems of assuring uniformity of dispersion forces throughout the fluid are discussed for each method. As an approximation, we have analyzed the changes in the average length as a function of time for several different fragmentation methods and reported apparent coefficients. More rigorous analyses are available if the distribution of energy is well known within the processing volume.

Gaussian distributions are often assumed to represent particle size distributions. However, we have found that MWNT length and diameter distributions are better described by log normal distributions, which have greater fractions of higher length scales than do Gaussian distributions. The interpretations of carbon nanotube fragmentation presented here are based on log normal particle size distributions, although the coefficients of Eq. (1) could be interpreted for other probability density functions as well.

Size Distribution Measurement and Analysis

It is possible to measure nanotube size distributions using SEM and optical microscopy. TEM is not useful for size distributions except when very short (<100 nm) tubes are present. Techniques for size distribution measurement are readily available in the literature. A probability density function needs to be fitted to the

experimental size distribution in order to obtain the distribution's moments and use Eq. (1). Fitting a differential distribution accurately might require as many as one thousand data points and is practical when digital imaging software can be applied to the problem. An alternative method is to determine the probability density function coefficients of cumulative particle size distributions for 50–100 nanotubes. This approach reduces the instrument time for length measurements and often provides sufficient accuracy for engineering models of the fragmentation process.

The MWNT lengths or agglomerate sizes were fitted with a log-normal model using Systat®. The differential probability density function has two fitting parameters, the standard deviation of the distribution, σ, and the logarithmic mean, μ.

$$f(\ln(L)) = \frac{1}{\sigma \cdot \sqrt{2\pi}} e^{-\frac{1}{2}\left(\frac{\ln(L)-\mu}{\sigma}\right)^2} \quad (2)$$

The cumulative probability distribution function of this distribution is the integral from negative infinity to $\ln(L)$ of Eq. (2)

$$F(\ln(L)) = \int_{-\infty}^{\ln(L)} \left(\frac{1}{\sigma \cdot \sqrt{2\pi}} e^{-\frac{1}{2}\left(\frac{\ln(L)-\mu}{\sigma}\right)^2} \right) d(\ln(L)) \quad (3)$$

Mechanical Methods

Ultrasonication

Ultrasonication of carbon nanotubes in solvents such as alcohols is a common technique for dispersing samples for electron microscopy. One way to improve the dispersion of nanotubes is to shorten the tubes. The shorter tubes are less likely to entangle and arrange into aggregates. However, there are some serious disadvantages with breaking the tubes into smaller pieces. When the tube-walls are broken in order to create a cut, the wall may become damaged in other ways as well. "Worm-eaten" or "ragged" tube walls.[150–152] and walls with cuts, buckles, and irreversible bends[153,154] are consequences of chemical processing, ultrasonication treatment or a combination of both methods.

Single-walled carbon nanotube lengths decrease only after the bundle size has gotten smaller.[155] Single-walled carbon nanotubes rearrange into super-ropes after the bundles are broken up and the SWNTs are shortened.[154,156] These super-ropes have diameters more than 20 times the initial bundle diameter. There have been attempts to develop less destructive ultrasonication methods. One example is ultrasonication with diamond crystals, a method that reportedly destroys the SWNT bundles but not the tubes.[157] Raman-spectra show typical SWNT peaks even after 10 hours of treatment with this method.

Ultrasonication creates expansion and peeling or fractionation of MWNT graphene layers. The destruction of multiwalled nanotubes seems to initiate on the external layers and travel towards the center. It has been reported that the nanotube layers seem quite independent, so MWNTs would not only get shorter, but actually thinner with time.[158]

Ultrasonication is an extremely common tool used to break up nanotube aggregates during purification, mixing, and other types of solution processing techniques. Therefore, the nanotube morphology in the suspension or solid is that developed during processing, and not that of the original nanoparticle additive. In some cases, ultrasonication can be used to remove impurities. Single-walled carbon nanotubes have been purified from ~70% to ~90% by ultrasonication-assisted filtration. About 30–70% of the starting material was not recovered in this process.[154] Ultrasonication also may lower nanotube quality. For example, ultrasonication lowers the oxidation onset temperature from 600°C to 500°C for MWNTs. This onset temperature is lower than for graphite, which is approximately 540°C.[158]

There are two major methods for delivering ultrasonic energy into liquids, the ultrasonic bath and the ultrasonic horn or wand. Ultrasonication disperses solids primarily through a bubble nucleation and collapse sequence.

The ultrasonication bath has a higher frequency (40–50 kHz) than cell dismembrator horns (25 kHz). Ultrasonication of fluids leads to three physical mechanisms: cavitation of the fluid, localized heating, and the formation of free radicals. Cavitation, the formation and implosion of bubbles, can cause dispersion and fracture of solids. The frequency of the ultrasound determines the maximum bubble size in the fluid. Low frequencies (about 20 kHz) produce large bubbles and high energy forces occur as they collapse. Increasing the frequency reduces bubble size and nucleation, so that cavitation is reduced. Cavitation does not occur in many liquids at frequencies larger than 2.5 MHz. The ultrasonication bath does not produce a defined cavitation zone as does a horn and the energy seems to be more uniformly dispersed through the liquid phase. Systems with low frequencies (20–100 kHz) and high power (100–5000 W) are used to modify materials.[159]

Bubbles nucleating at solid surfaces and rapidly expanding can push particles apart. Solid particles can remain separated after bubble collapse if they are wetted

by the fluid phase and if the volume fraction of nanoparticles in the fluid phase is low enough so that solid movement is possible.

Bath Ultrasonication

Multiwalled carbon nanotubes (wall material) were dispersed in toluene by using an ultrasonication bath (a frequency of ~55 Hz). The MWNTs had initial dimensions of $L = 50\,\mu m$, $D_i = 2.9$ nm and $D_o = 25$ nm, respectively. Water in the ultrasonication bath was kept at the same level as the toluene in the 200 mL glass beaker, thus promoting a uniform energy distribution. The MWNT loading was 0.1 wt.%, and samples were taken from the bath after 5, 10, 15, 20, and 25 min. Each sample was analyzed by using SEM (Hitachi 3200N Variable-Pressure SEM). Ten SEM microphotographs were taken of each sample and from these a minimum of a hundred MWNT lengths were measured.

The measured MWNT lengths were plotted cumulatively and modeled using equations (2) and (3) from above. Figure 12 compares the distributions of the time sequence samples. The log-normal models are also presented in the differential form in Fig. 13 and the model parameters are presented in Table 5. Equation (3) was fitted to the mean average length data (Fig. 14). The change in average length during the first few minutes of sonication is dramatic. After the first 5 min, the average length is reduced from 50 to 17 μm, a decrease of more than 65%. After processing for an additional 20 min, the MWNT average length decreased to 6.5 μm. This result is not unexpected, since it takes more energy to break shorter, more stable, tubes. The average length data are well-described by a model that is cubic in length ($k_b = 3.55 \times 10^{-4}$, $b = 3$). The differential curves (Fig. 13) clearly show the loss of larger tubes at longer sonication times.

Ultrasonication Horn

The tips of ultrasonic wands oscillate at a fixed frequency with variable power being applied to the fluid phase. The rapid oscillation of the wand tip produces a conical field of high energy in the fluid. The solvent within this conical field undergoes nucleated boiling and bubble collapse, which is the

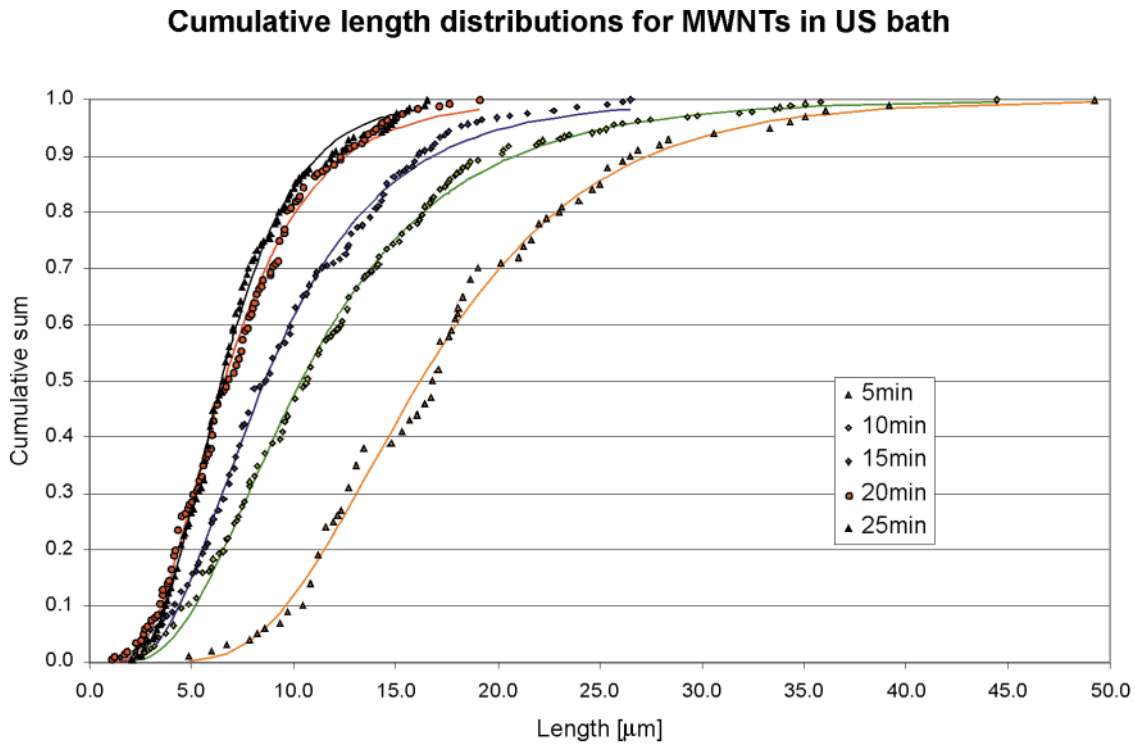

Figure 12. Cumulative MWNT length distribution as a function of processing time in ultrasonication bath. The initial distribution changes are quite dramatic, while the changes are more moderate after a longer treatment period.

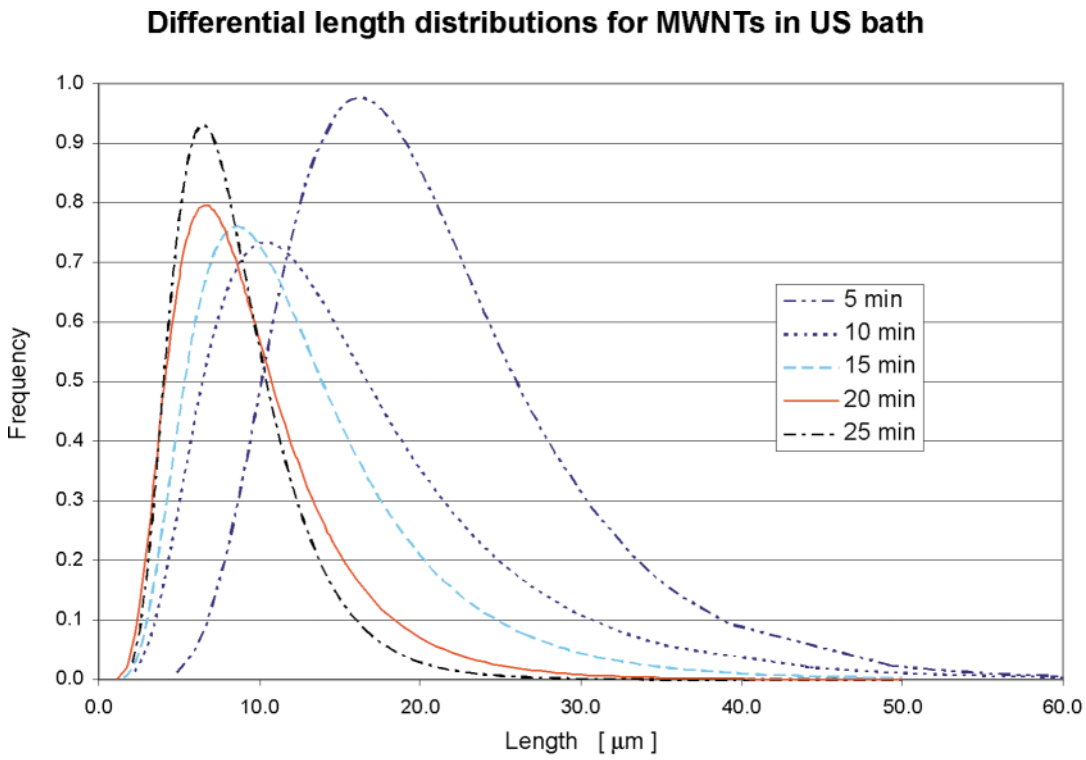

Figure 13. The normal density function for MWNT lengths. MWNTs treated with an ultrasonication bath for 5, 10, 15, 20, and 25 minutes respectively.

primary mechanism by which ultrasonic energy disperses materials. The wand tip vibrations along with the rapid generation and collapse of bubbles induces a flow that moves away from the wand tip and then recirculates through the conical zone again. The size of the zone and the local velocity fields depend on the boiling point of the solvent, the fluid phase viscosity, the energy applied, and the geometry of the vessel and the wand placement.

Table 5. Multiwalled carbon nanotubes treated in ultrasonication bath.

Time (min)	Mean length (µm)	Standard deviation
5	16.2	0.41
10	10.4	0.54
15	8.6	0.52
20	6.6	0.50
25	6.5	0.43

Note: The MWNT mean length and standard deviation are the model parameters used to fit the log-normal model to the data. The initial MWNT average length was 50 µm.

The volume fraction of nanotubes in the suspension affects the solid surface per fluid volume. Fluids with high continuous phase viscosities, for example, polymer solutions and spinning dopes, may not give rapid recirculation of the process liquid through the sonication zone. Since suspensions of MWNTs are shear thinning,[160] the flow field near the wand tip may be only a small volume and may have low recirculating velocities through the sonication zone, leading to low dispersion efficiencies. Multiwalled carbon nanotubes suspensions with polymer solutions as the continuous phase may also have greatly reduced fluid circulations near the wand tip. Not all the bubbles may collapse immediately, particularly if the solvent does not wet the nanotubes well or if a polymer solution continuous phase of high viscosity reduces the rate of bubble coalescence. At high solids loadings, the nanotubes can trap gas bubbles and create a rigid network that prevents fluid flow.

Dispersion of 0.1 wt.% dispersion of MWNTs in toluene were treated with an ultrasonication horn. Data were collected and modeled in the same manner as above. Figures 15 and 16 show the cumulative and differential size distributions, respectively. The data are presented in Table 6. Figure 17 shows the fit of Eq. (3) to these data ($k = 4.06 \times 10^{-4}$, $b = 3$). The data are well-

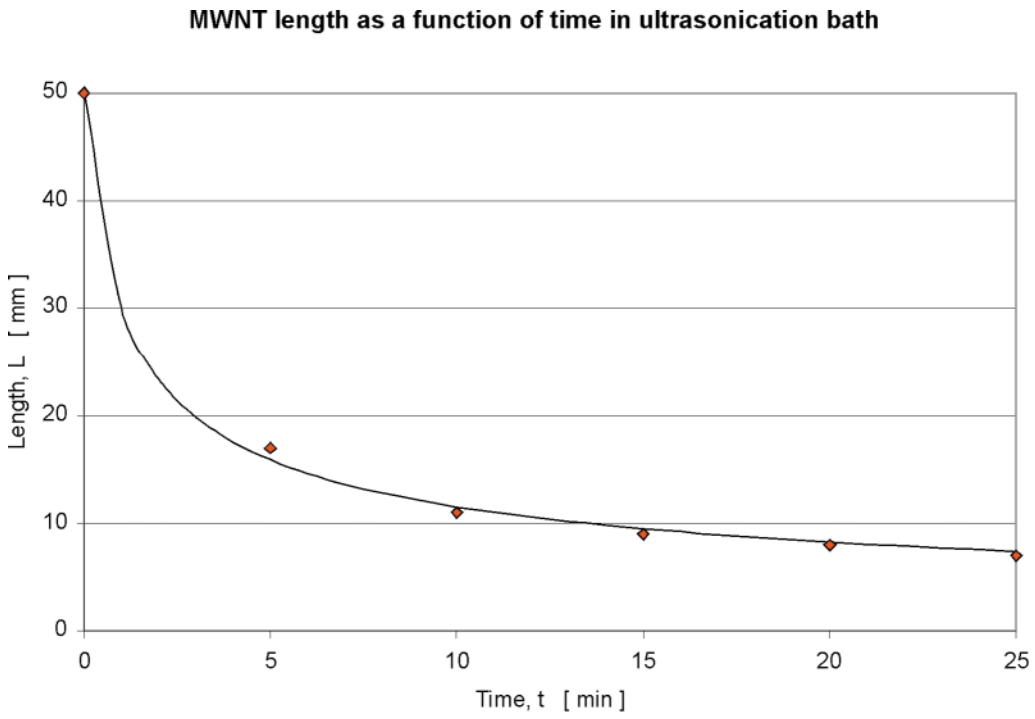

Figure 14. The time derivative of MWNT length in US-bath. The data is fitted with a power model where the frequency factor, k, is 3.55×10^{-4} and the exponential parameter, b, is 3.

described by a cubic model, but with a slightly different rate coefficient. The difference between the sonication frequencies may account for some of this change.

Orientation of Nanotubes in Polymers

In some cases, it is desirable to align the nanotubes in a composite, a process that requires the tubes to be well separated. It is possible to align SWNTs in poly(urethane) or poly(acrylate), either by shear flow prior to polymerization or by stretching the already cured matrix.[161] There have also been attempts to align MWNTs in PHAE by means of stretching.[162,163] The films were stretched up to 500% and no broken tubes were detected, even though some tube buckling was observed. In addition, it is possible to align carbon nanotubes by taking advantage of their electrical conductivity. One research group dispersed carbon nanotubes in ethanol in a DC-field (250 V/mm) for half a minute. Tube alignment was observed and moreover longer tubes were collected at the cathode, which means that the method can be used for purification and size-grading of nanotubes.[164] Single-walled carbon nanotubes shortened by ultrasonication ($l = 20$–100 nm) have also been aligned along a HOPG-lattice (highly oriented pyrolytic graphite). The film showed a semiconductive behavior.[165] Solvent casting and melt-mixing of SWNTs and PMMA in a hot-press has also been used to promote nanotube alignment. Higher electrical conductivity was detected in the flow direction (0.118–11.5 S/m) than that in the perpendicular direction (0.078–7 S/m).[135]

Ultrasonication of Multiwalled Carbon Nanotubes in Polyacrylonitrile Spinning Dope

An example of the importance of MWNT dispersion to a process result is the development of continuous fibers containing carbon nanotubes. Such systems could be used as high strength fibers, and for fibers with high toughness. The use of high aspect ratio solids in spun fibers will depend on uniform, independent particle dispersions, proper orientation of the fibers in the spinneret or die, and drawing to develop fiber strength. Poor dispersion will result in unspinnable polymer dopes.

Weisenberger[166] studied the spinning of PAN dopes loaded with MWNTs for producing MWNT/PAN fiber composites. A cell dismembrator (horn ultrasoni-

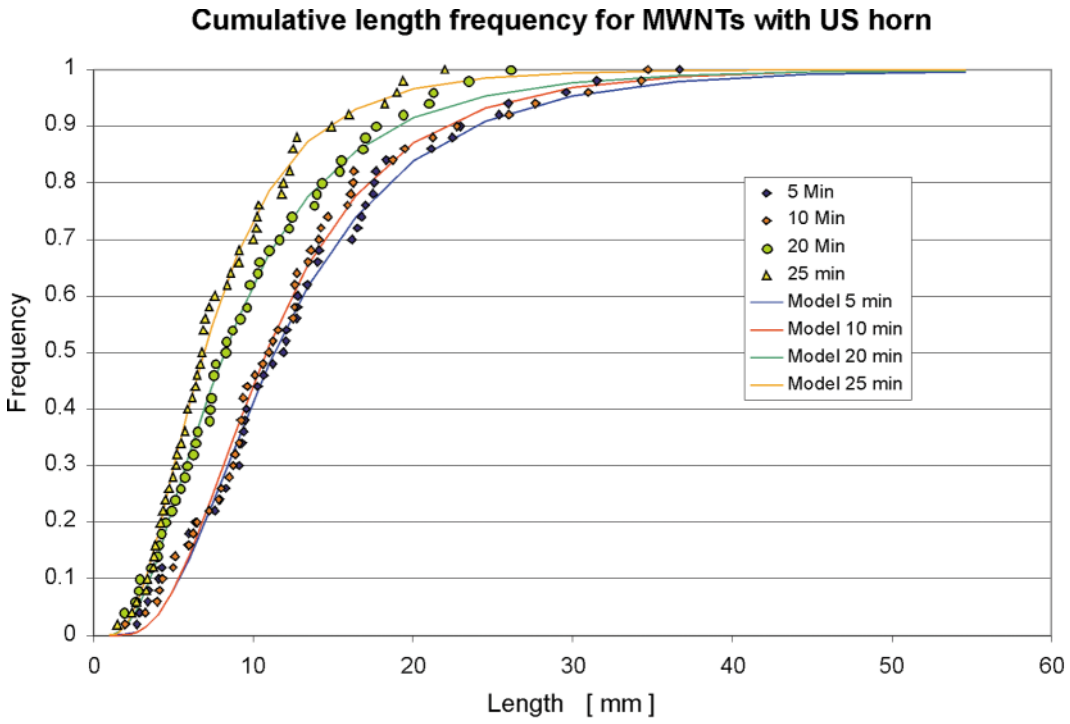

Figure 15. Plot showing the cumulative MWNT length distribution as a function of processing time with ultrasonication wand.

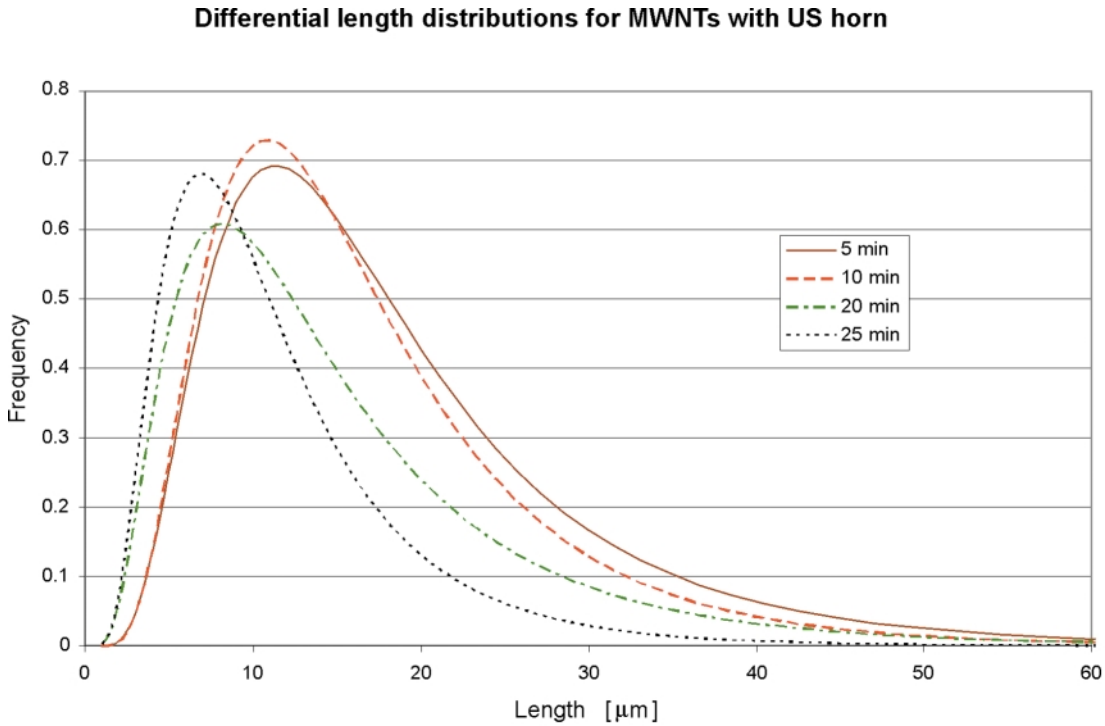

Figure 16. The normal density function for MWNT lengths. MWNTs treated with an ultrasonication wand for 5, 10, 20, and 25 minutes respectively.

Table 6. Multiwalled carbon nanotubes treated with ultrasonication horn.

Time (min)	Mean length (μm)	Standard deviation
5	11.4	0.58
10	10.8	0.55
20	8.2	0.66
25	6.9	0.59

Note: The MWNT mean length and standard deviation are the model parameters used to fit the log-normal model to the data. The initial MWNT average length was 50 μm.

cation at 25 kHz) was used to disperse MWNTs into a solvent (dimethyl acetamide) before adding polymer to form the spinning dope. The sample was cooled in an ice bath to remove excess heat. The fluid was sonicated at 300 W of power for 10 second intervals over various time periods to produce well-dispersed suspensions for spinning. The quality of the dispersion was evaluated by determining whether the dope prepared from the suspension could be spun into continuous fibers. Figure 18 shows the energy per unit volume needed to produce MWNT dispersions that could be spun into viable fibers. The energy per unit volume for good dispersions increases as the weight fraction of nanotubes in the liquid phase increases. The extrapolation of the linear model to zero weight fraction nanotubes suggests that a significant amount of energy is dissipated into heat or fluid motion, rather than nanotube dispersion. Empirical models relating mixing energy per unit volume to the quality of particle dispersions have been used in many polymer compounding applications, such as the dispersion of carbon blacks in elastomers. Figure 18 could be used to develop reproducible MWNT dispersion processes.

Insufficient dispersion of the MWNT resulted in dopes that were not spinnable. Typically, poor dispersion gave extrudates with a grainy surface that would not drawdown in a homogeneous fashion. Numerous fiber breakage events would occur during spinning, and a characteristically visible rough fiber surface would form. However, the nanotube length distribution was essentially the same after spinning compared to before, as presented in Figs. 19, 20, and Table 7. Figure 21 shows cross-sections of PAN fibers with nanotube agglomerates, which reflect light and appear white in the photomicrograph. The nanotube agglomerates cannot align with the fiber axis during the elongational flows of the spinning and drawdown processes, in contrast to individually separated nanoparticles (Fig. 22).

High Impact Mixing—Ball-Milling

Ball-milling has been used to narrow the length and diameter distributions[167] and to open the nanotubes[168,169] for improved sorption capacity for gases. However, it has also been observed that a large amount of amorphous carbon is created,[157,169] which clearly indicates that the tubes are damaged in different ways and that ball-milling is a destructive method. The creation of amorphous carbon introduces a high surface area, which is a more likely explanation to the increased storage capacity than the introduction of open tube ends would be.[4,157,170] Bending, defects and tube–tube contacts strongly modify the electrical behavior of carbon nanotubes. Structural topological defects always increase the resistance of metallic nanotubes, making it dependent on the defect density per unit length.[171]

Some groups have tried to produce boron nitride nanotubes and carbon nanotubes from graphite through ball-milling. The iron from the mill balls functions as a catalyst and the heat becomes elevated through the mechanical impact, so the process parameters are in the right region, but the results have not been impressive.[172–175] In addition, the created nanotubes are destroyed after a longer period of milling.

Ball-milling has also been used in an attempt to intercalate lithium in SWNTs, creating compounds to be used in batteries.[176] Li-intercalated graphite and carbonaceous materials are commercially used in Li-ion batteries.[177,178] The intercalation involves electron donation from the alkali metal to the nanotube. The same type of experiments have also been carried out with K, Rb, Cs on both SWNTs and MWNTs.[179–184]

Grinding and Rubbing

There are few reports on the subject of rubbing or grinding carbon nanotubes to decrease the size. Rubbing is more destructive than any other method. The process introduces cuts and bends in SWNTs, but no change in storage capacity is observed.[157] A less damaging method is chemically cutting SWNTs by grinding them in a fluid (α- or β-cyclodextrin) using mortar and pestle. Both tube lengths and bundle diameters were noticeably reduced. Other grinding agents were used as well, but did not give as good results; samples contained mostly long tubes.[185]

MWNTs can be hand-ground with mortar and pestle. The MWNTs were mixed with a small amount

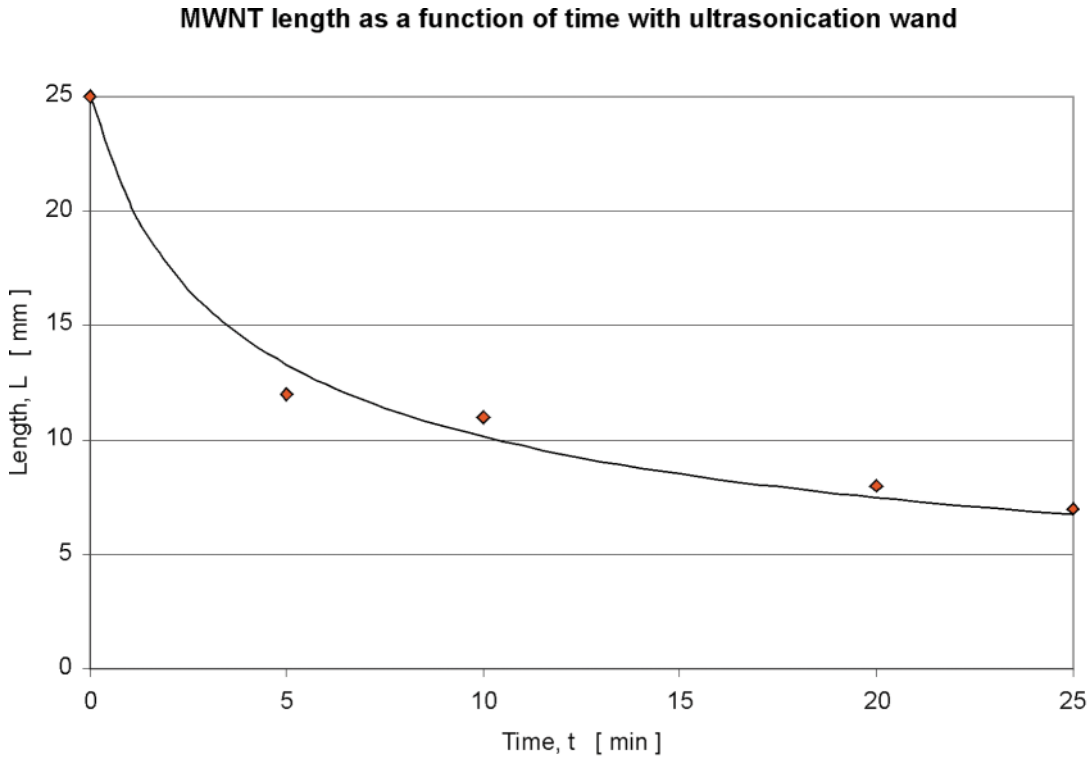

Figure 17. The time derivative of MWNT length in US-bath. The data is fitted with a power model where the frequency factor, k is 4.06×10^{-4} and the exponential parameter, b, is 3.

of toluene, creating a thick paste. The paste was ground for approximately an hour, with no further addition of toluene. The MWNT length and diameter were measured before and after the grinding, using a Hitachi 3200N Variable-Pressure SEM. In addition, the MWNT agglomerate particle sizes were measured as well (MWNTs from the CVD process are entangled as harvested from the reactor and are associated into agglomerates). The data were fitted using the log-normal model, as described above. Different loadings of ground MWNTs were

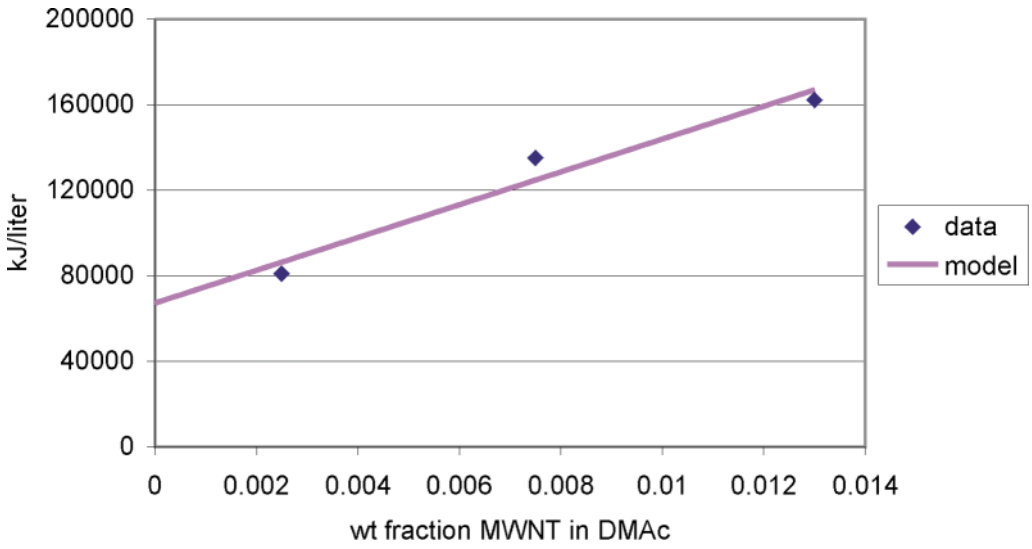

Figure 18. Ultrasonic energy required for dispersion of MWNTs in spinnable PAN dopes. *Source*: Ref. 166.

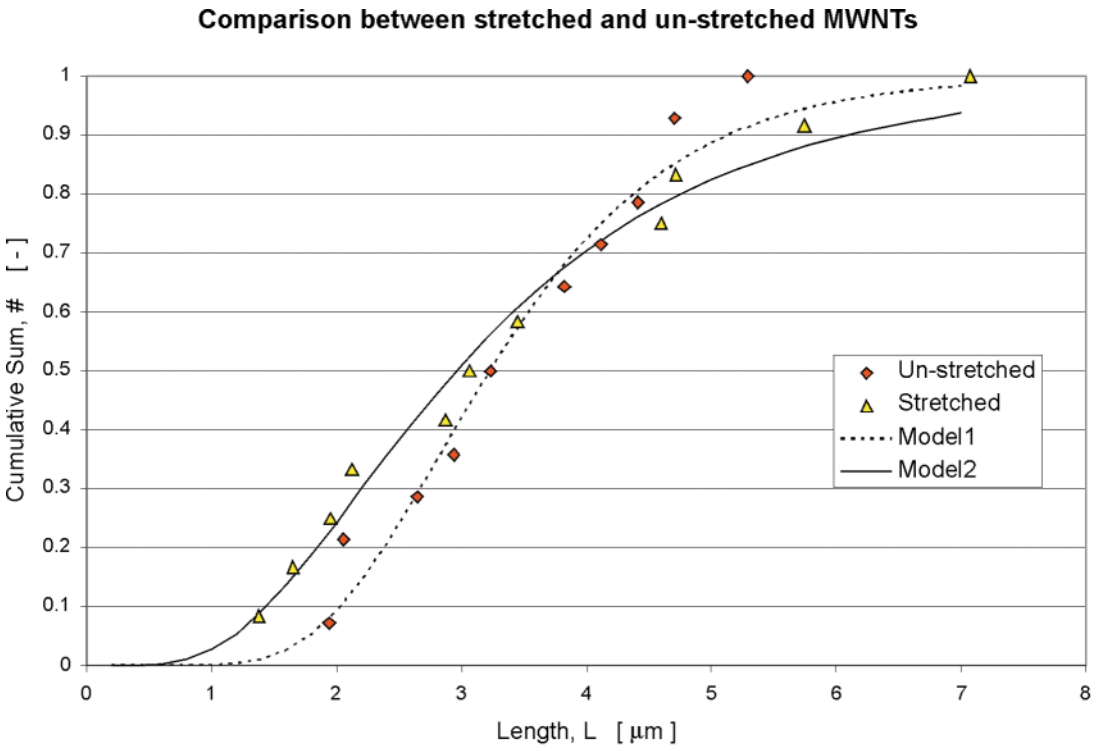

Figure 19. Cumulative distribution of MWNTs from spun and drawn MWNT/PAN fibers.

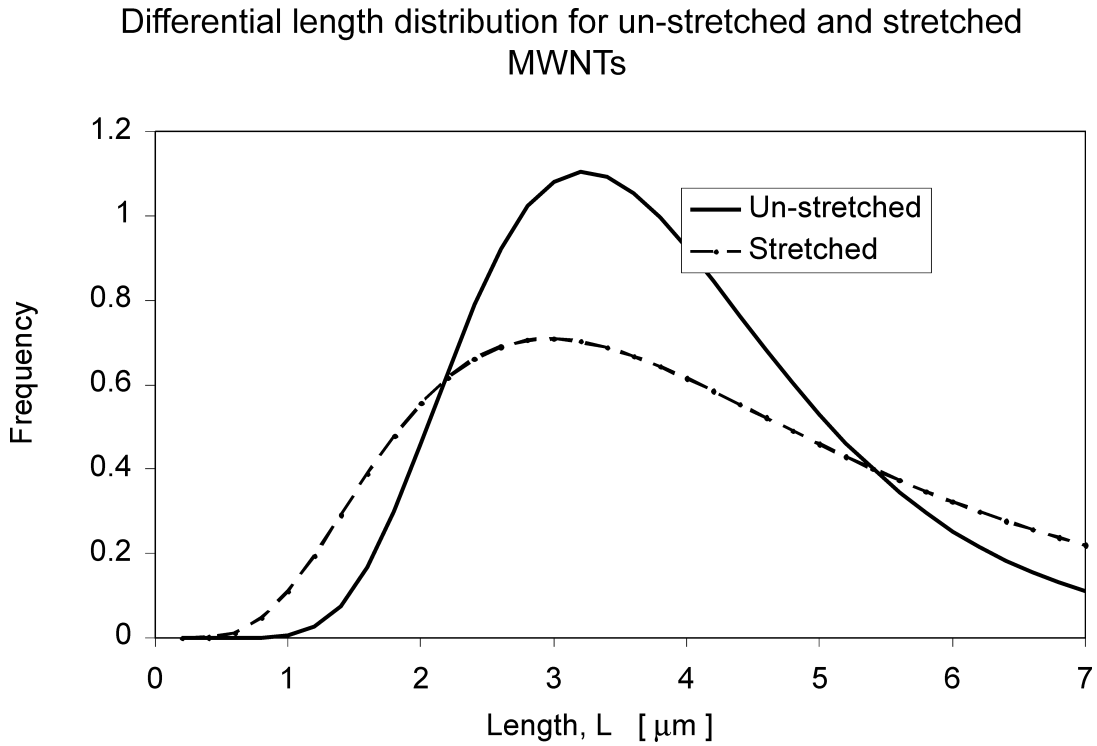

Figure 20. Differential distribution of MWNTs from spun and drawn MWNT/PAN fibers.

Table 7. Comparison of MWNT lengths of spun and drawn samples.

Sample	Mean length (μm)	Standard deviation
Un-stretched	3.2	0.36
Stretched	3.0	0.56

blended into epoxy-resin. The epoxy–MWNT blends were analyzed using a light microscope, to confirm a homogeneous blend, then used as contact cement between copper-covered strips of circuit board. After the polymer-blend had been cured, the electrical resistance was measured.

Both the lengths and agglomerate sizes decrease significantly, as seen in Figs. 23, 24 and 25. Figure 23

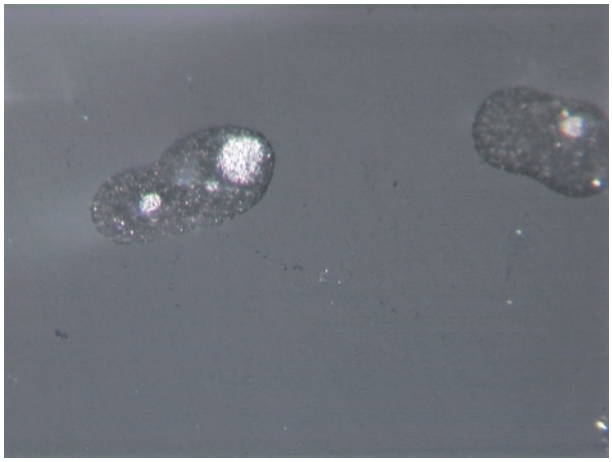

Figure 21. MWNT agglomerates in PAN fibers. The fiber diameters are about 25 microns. *Source*: Ref.[166]

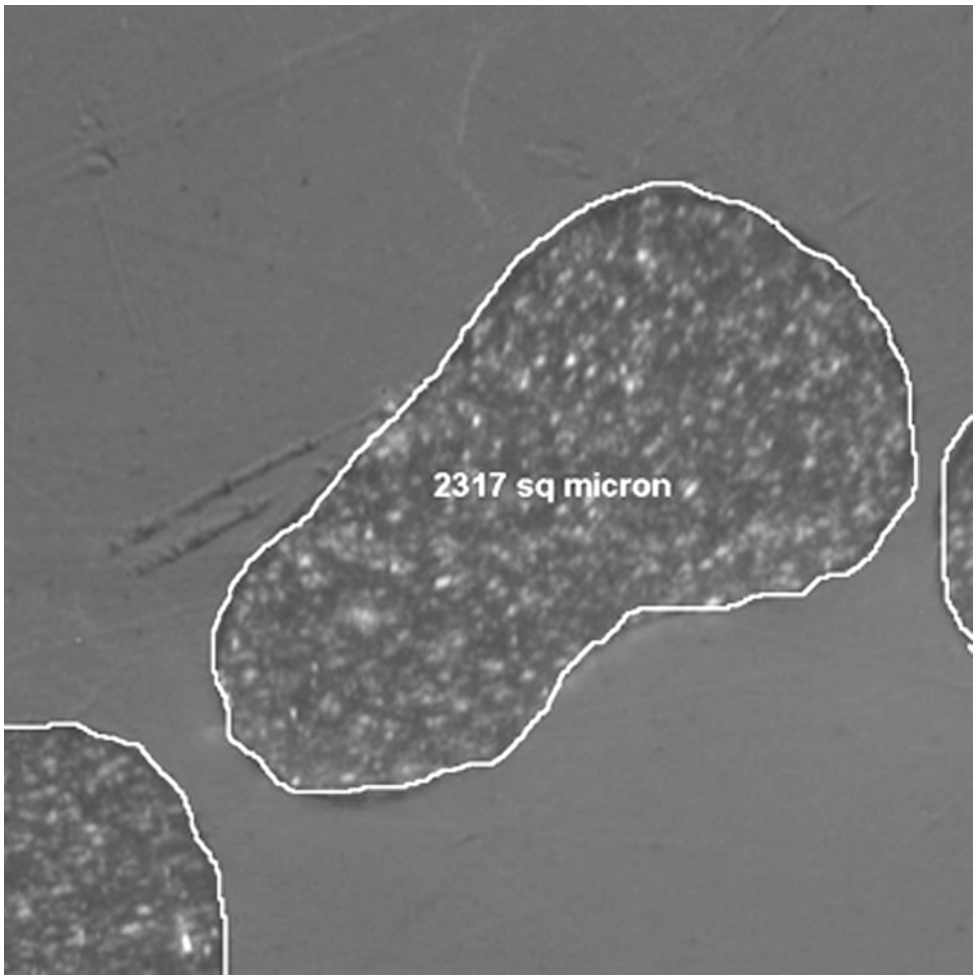

Figure 22. Fracture surface of MWNT/PAN fibers at 1 wt.% loading. Fiber surfaces are smooth, and the nanotubes are oriented along the fiber axis. *Source*: Ref.[166]

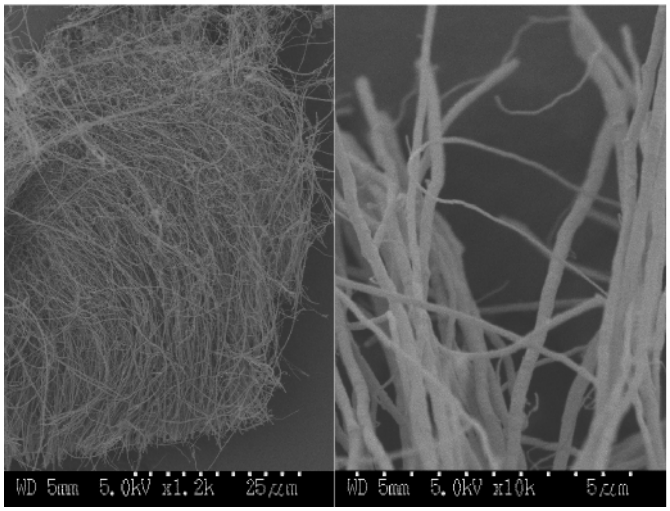

Figure 23. MWNT lengths before mechanical grinding with mortar and pestle.

shows the aligned nanotubes prior to grinding, showing uniform lengths, but variable MWNT diameters. Figure 24 shows a dramatic length decrease of the nanotubes. MWNT aggregates exist before and after grinding: the aggregate average diameter decreases by a factor of 5, as can be seen in Figure 25. The MWNT inverse aspect-ratio is presented, together with the fitted log-normal model, in Fig. 26. The change in aspect-ratio is shown due to its impact on the percolation theory. The diameter, length, and agglomerate size distributions before and after grinding, accompanied by respective fitted log-normal model curve, are presented in Figs. 27, 28, and 29, respectively. The MWNT diameter distributions are relatively unchanged by the grinding process. The length distribution changes from nearly monodisperse ($L = 55$ microns) to a log normal distribution with an average length of 3 microns. The typical agglomerate size was reduced from 170 microns to 40 microns.

Grinding produced significant defects in the MWNTs, as can be seen in Figures 30 through 32. Figure 30 shows a bent MWNT, with crimping on the curved inner radius. In Fig. 31, a partial tear along the radial direction is shown, and Fig. 32 shows the exfoliation of an outer layer of the MWNT. While much of the mechanical energy goes into complete breaks of the tubes, new defect sites are continuously generated on the tube surface.

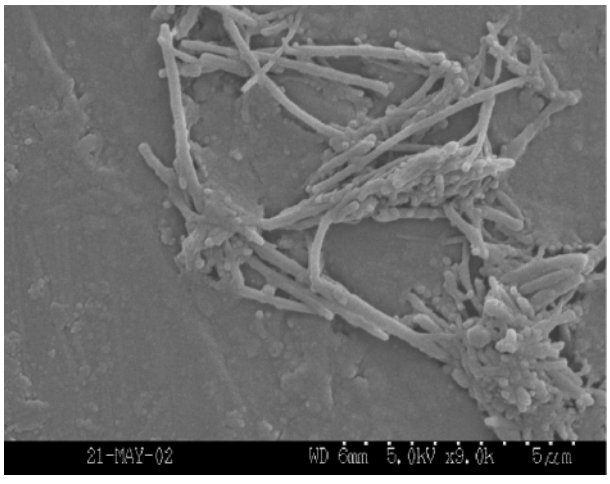

Figure 24. MWNT lengths after mechanical grinding with mortar and pestle.

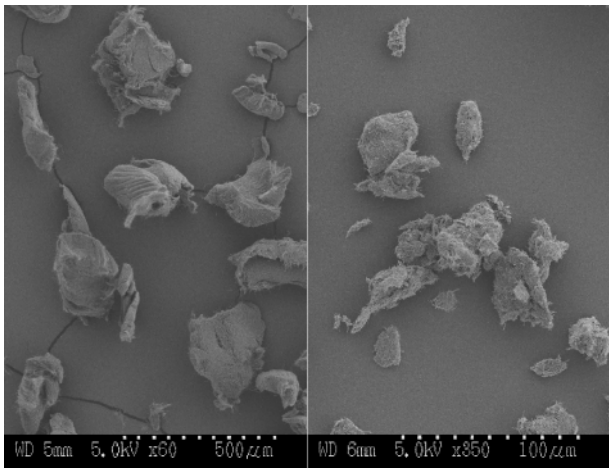

Figure 25. SEM microphotographs showing the diameter decrease for MWNT agglomerates after approximately 1 hour of mechanical grinding with mortar and pestle. Observe the different scales of the different halves.

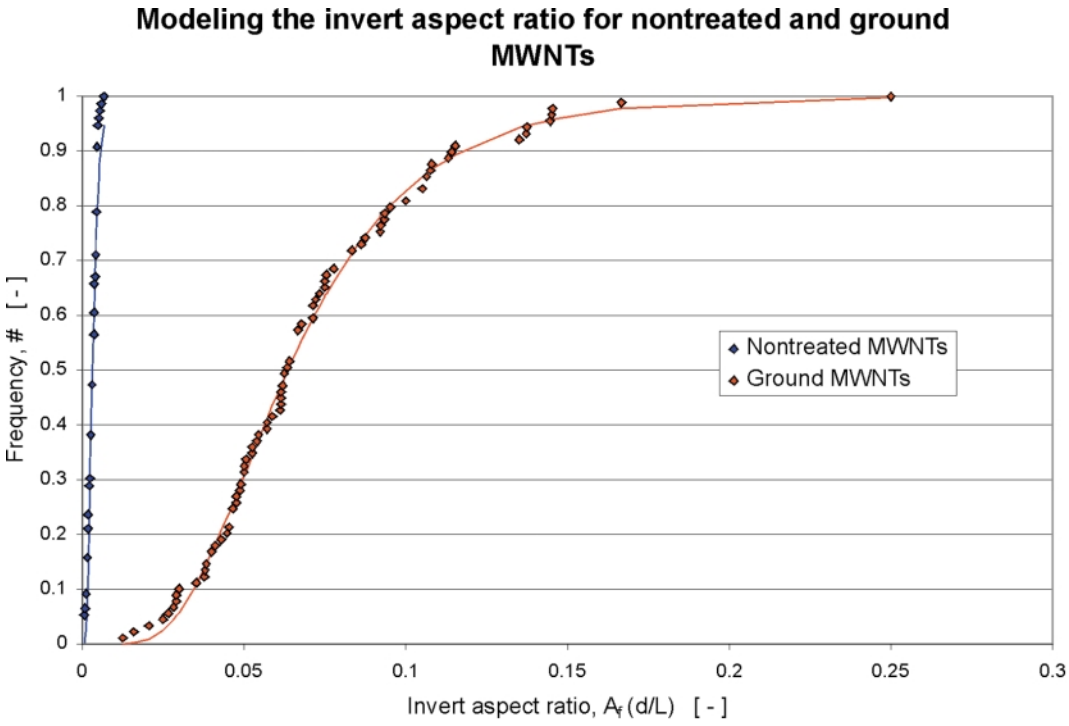

Figure 26. Cumulative distribution of aspect ratios for ground and unground MWNTs. Parameters are $d/L = 3.1 \times 10^{-3}$; $\sigma = 0.48$ for nontreated MWNTs, and $d/L = 6.4 \times 10^{-2}$, $\sigma = 0.48$ for treated MWNTs.

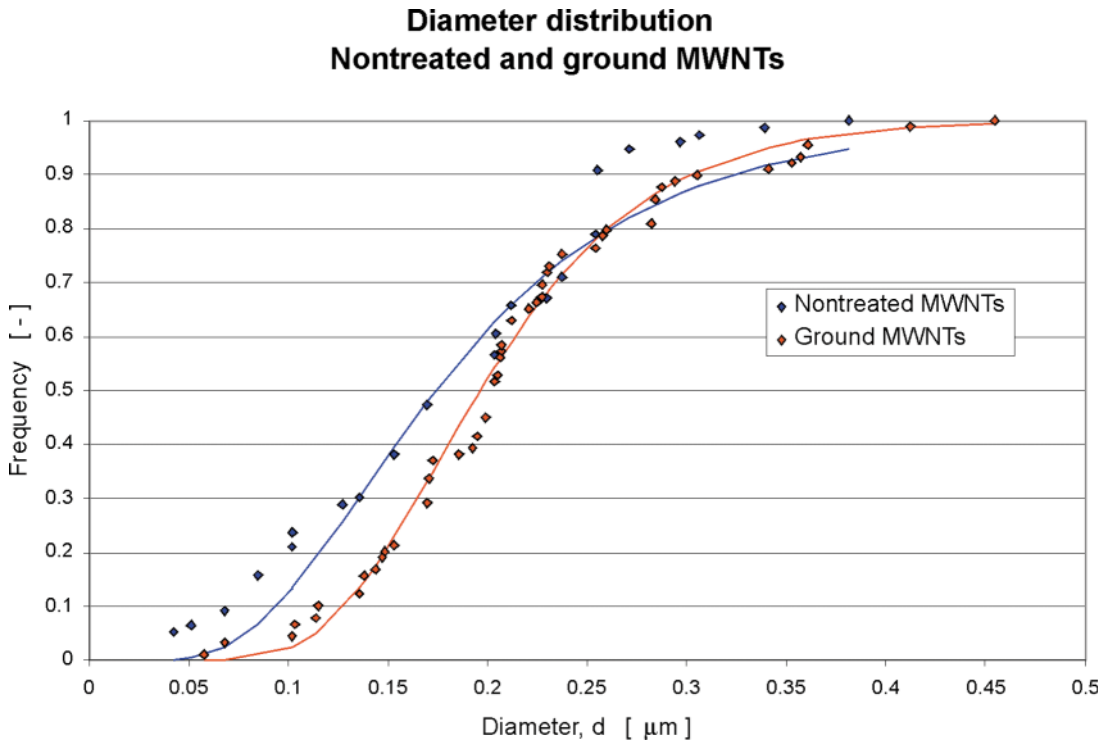

Figure 27. Cumulative distribution of MWNT diameters for ground and unground MWNTs. Model parameters are $d = 0.17\,\mu m$, $\sigma = 0.48$ for nontreated MWNTs, and $d = 0.20\,\mu m$; $\sigma = 0.34$ for ground MWNTs.

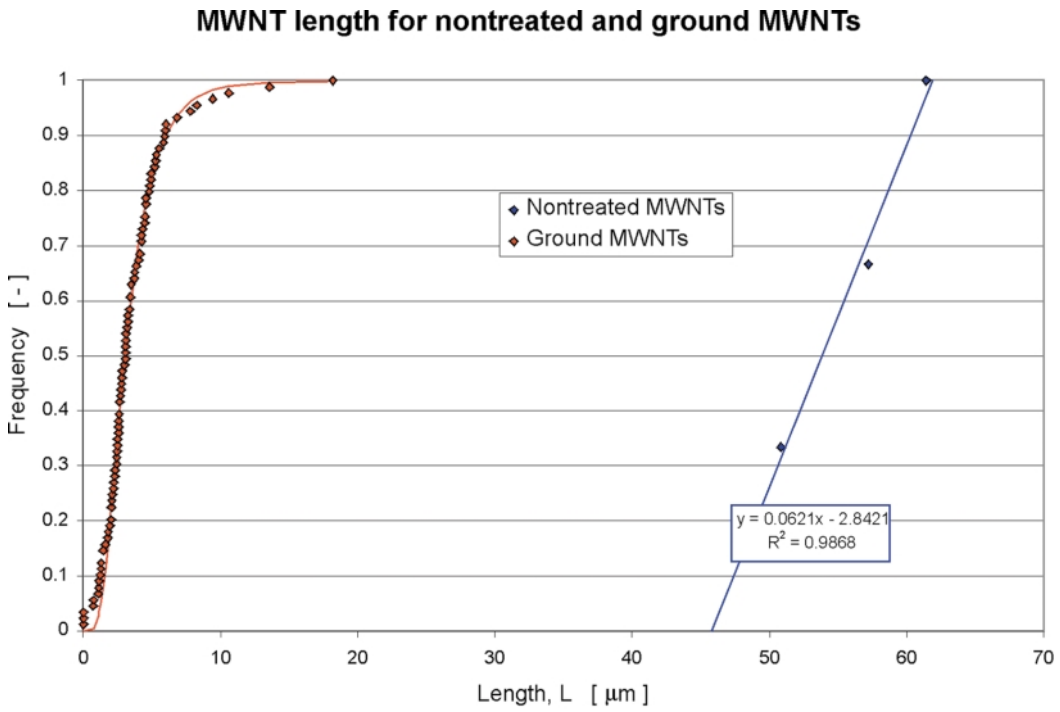

Figure 28. Cumulative distribution of MWNT lengths for ground and unground MWNTs. Model parameters for ground nantubes are $L = 30.3\,\mu m$, $\sigma = 0.53$.

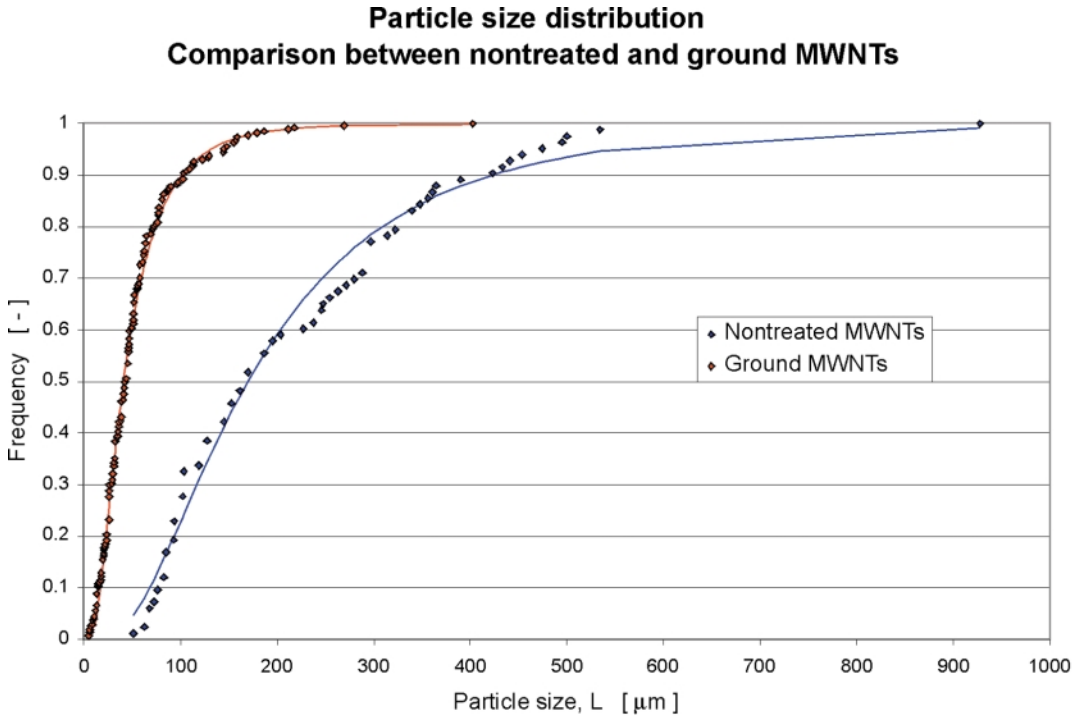

Figure 29. Cumulative distribution of particle sizes for ground and unground MWNTs. Model parameters are $d = 169.3\,\mu m$, $\sigma = 0.71$ for nontreated MWNTs, and $d = 40.6\,\mu m$, $\sigma = 0.71$ for ground MWNTs.

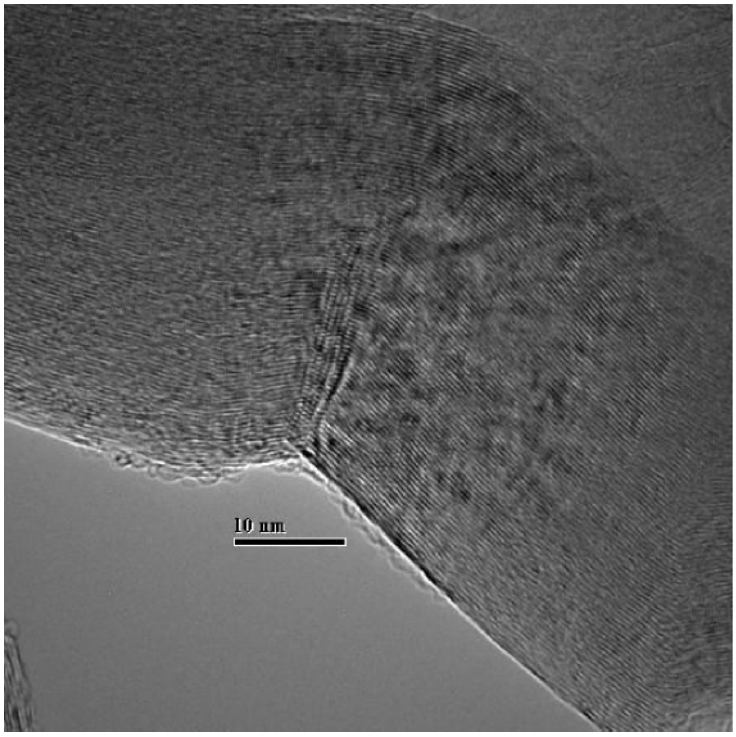

Figure 30. A bent MWNT, with crimping on the curved inner radius.

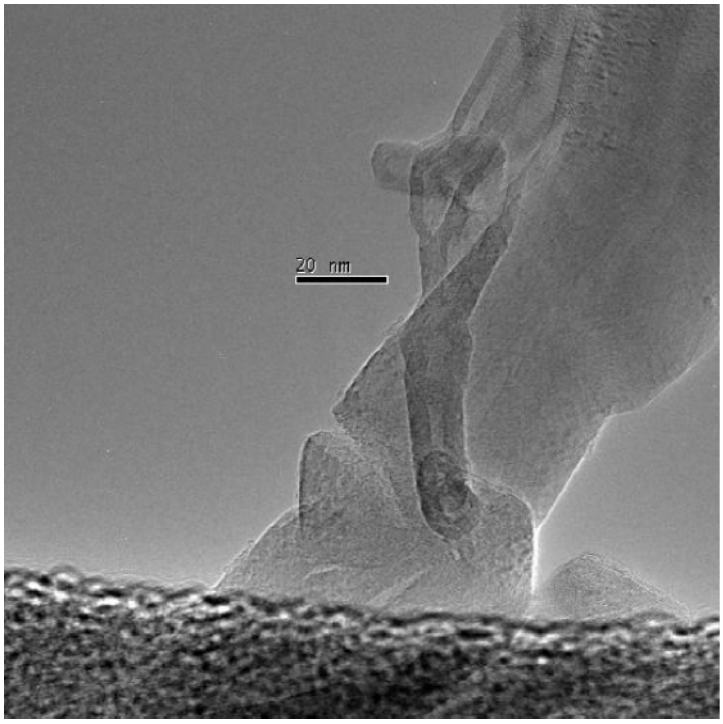

Figure 31. A partial tear along the radial MWNT wall direction.

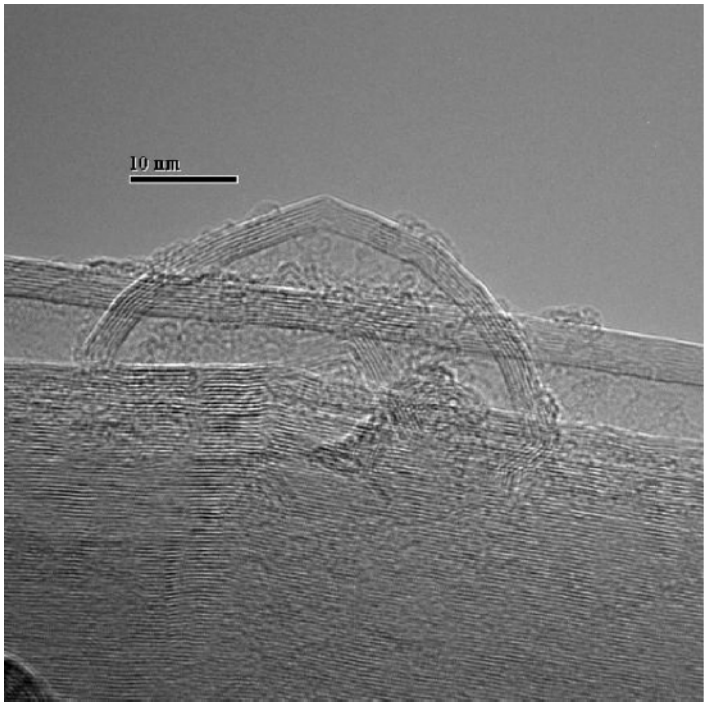

Figure 32. Delamination of an outer layer of the MWNT wall.

High Shear Mixing—Shear Stress Through a Nozzle

Another mechanical method is to apply shear force to pull agglomerates apart—high shear mixing. Usually narrow passages, and/or relatively high rates of flow, are required to generate high shear; in a lot of cases, rotor and stator construction is used. In our experiment, we applied a diesel fuel injector to create the high shear.

The fluid is passed through a diesel injector nozzle at a shear rate that causes the less shear stable materials, mostly polymer molecules, to degrade. In the lubricant industry, it is called fuel injector shear stability test (FISST), with an ASTM designation as D5275. The objective of this experiment is to find out the shear stability of the carbon nanotubes in oils compared with that of polymer molecules.

Carbon nanotubes were dispersed into a synthetic oil, four centistokes poly(α-olefin) with the aid of a nonionic dispersant. Kinematic viscosity was measured at 40°C and 100°C using a Cannon-Fenske viscometer. Because the dispersion is completely black even with the addition of only 0.005 wt.% carbon nanotube, the reverse flow tube was used. The test fluid is pumped through a small-clearance diesel-injector nozzle, which provides both turbulent and localized shear. In the test, the apparatus is first flushed with three separate 100 mL portions of the test fluid, and then 100 mL of the test fluid passes the nozzle for 20 cycles. After the completion of the 20 cycles, the sheared fluid was collected, and viscosities at 40°C and 100°C before and after shear were measured and the shear viscosity loss was calculated.

Figure 33 shows the plot of kinematic viscosity vs. the weight percentage of carbon nanotube. The viscosity profile of the nanotubes is very similar to that of the cylindrical particle suspensions, indicating that at certain point the carbon nanotubes can be treated as high-aspect-ratio cylindrical particles. Further studies are necessary to model the viscosity profile of this system. The 0.05 wt.% nanotube dispersion is then used for the shear nozzle test, and the results are summarized in Table 8.

It can be seen that the viscosity of the system decreases dramatically after the test. As a matter of fact, 50% viscosity loss at 40°C has never been observed for a commercial motor oil before. It indicates that the carbon nanotubes dispersed in the medium have been sheared into "broken pieces". Figure 34 shows the scanning electron microscopic pictures of the sample before and after the shear nozzle experiment. It is evident that, after shear, the networked structure in the previous dispersion is destroyed, and the aspect ratio of the remaining tubes becomes smaller.

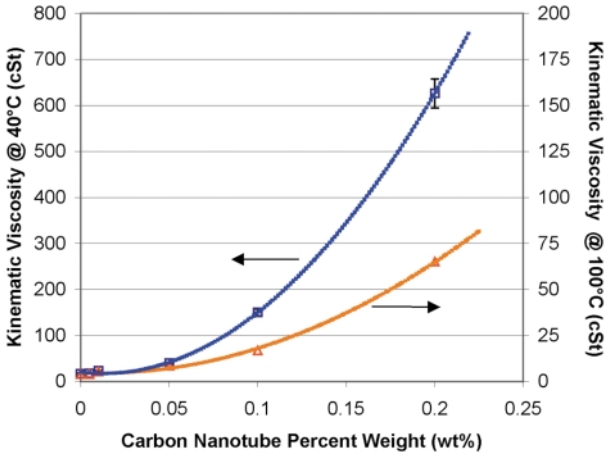

Figure 33. Kinematic viscosity of the dispersions of carbon nanotube in poly(α-olefin) at various concentrations.

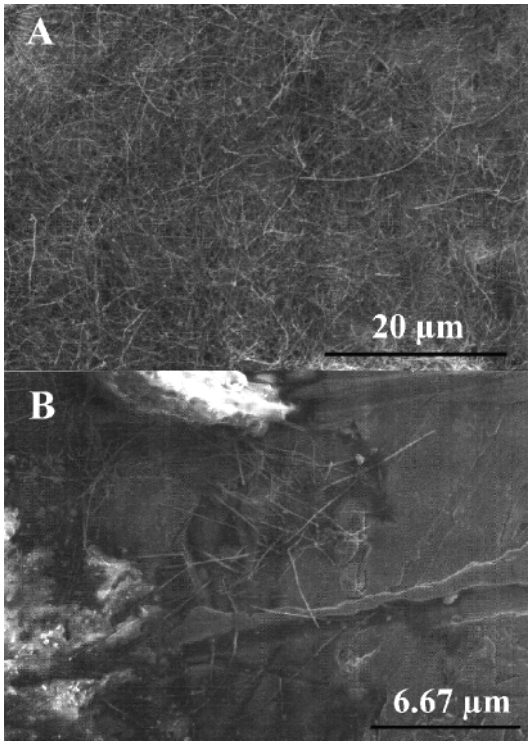

Figure 34. SEM pictures of the 0.05 wt.% nanotube dispersion. (A) Before FISST; (B) After FISST.

Chemical Methods

If the carbon nanotube surface is modified through functionalization, the interaction between the tube and the surroundings is affected. By choosing a specific type of functional group, it is possible to influence the interaction in different ways. This treatment may enhance nanotube dispersion in different solvent and polymer systems, allowing flexibility in creating novel hybrid composites. For example, by covalently attaching alkene groups to SWNT side-walls, the solubility in various organic solvents,[186–189] such as THF, chloroform, methylene chloride,[190] and DMF,[191] increases. The nanotubes can also be co-polymerized in a polymer matrix as a block, graft or crosslinked polymer.[192,193] A brief review of functionalization methods investigated is given below.

Acidic Treatments

Acid treatment in combination with thermal oxidation or decomposition, is a very common way to purify both MWNTs and SWNTs.[194,195] Usually the nanotubes are boiled or soaked in acid for time-periods of hours or even days and thereafter burned in oxygen or air, pure or mixed with other gases. In the first step, the catalytic metal particles that are left in the sample are eliminated, and in the second step unwanted carbon, such as amorphous carbon and carbon particles, are consumed. Oxidation may separate SWNTs into individual fibers.[196,197] Furthermore, oxidation also cuts the nanotubes in sites with high structure damage or defect density, which leads to the production of shorter nanotubes[198–200] with a higher morphological quality. Also, thinner tubes are usually more reactive than tubes with a larger diameter, due to the greater strain on the bonds in the thinner tubes.[201,202] It has been observed that when MWNTs are boiled in acid, their diameters decrease. This mechanism is pronounced for tubes with stronger curvature. A molecular dynamics study suggests that there might be negative effects from chemical modifications of SWNT. For small tubes, the strain can cause the functional groups to dissociate. The helical conformation has little impact. Furthermore, introduction of sp^3-hybridized carbon due to chemical functionalization does degrade the strength of SWNT by ~15%.[82] This also explains why the nanotube active sites are theoretically

Table 8. Comparison of suspension viscosity before and after high shear spraying through a nozzle.

	40°C	100°C
Viscosity before shear	40.09 cSt	8.59 cSt
Viscosity after shear	19.72 cSt	5.40 cSt
Viscosity loss, %	50.8	37.1

concentrated on the end caps,[203] where the tube geometry presents its largest curvature. In one investigation, Raman-spectra show that functional groups of acidic nature, such as —C═O, —COOH, and —OH, were attached to the tube ends. After a sufficient period of boiling (2 hours) the sample could not reach pH = 6 when washed in de-ionized water, since the nanotubes could not precipitate due to the attractive forces between the acidic groups and H_2O. Furthermore, 18% of the sample had been consumed at this time. If nanotubes are ultrasonicated in HNO_3 or HNO_3/H_2SO_4, acidic functional groups are created as well. Also in this case, the functional-group quantity is time-dependent. The oxygen concentration is eight times higher for treated tubes than for non-treated tubes.[153]

Successful openings of nanotube ends have been performed using oxidants, such as HF/BF_3 and OsO_4. In addition, the tubes were filled with metals and the ends were closed again, or covered, by reduction with benzene in Ar or H_2, or with reagents such as ethylene glycol.[204] For SWNTs, it has been reported that it is possible to achieve a purity of >95% with a yield of 20–50%.[205,206] The purification yield was reported at 54% for MWNTs.[206]

Oxidation can be carried out both in liquid-phase and in gas-phase. Investigations suggest that primarily hydroxyl and carbonyl groups are formed during gas-phase treatment of MWNTs, while liquid-phase treatment forms carboxylic acid groups.[207] It has also been seen that SWNTs treated with HNO_3/H_2SO_4 or H_2O_2/H_2SO_4 mixtures produces both carbonyl and ether functional groups.[208] It is possible to remove the groups by thermal decomposition in vacuum. Ethers and quinines are harder to remove than carboxylic acid groups.

The acidic surface sites that are created on the nanotube surface are reactive and act as nucleation sites functionalizing the tubes in other ways. One example is the decoration of nanotubes with nanoscale metal clusters (Au, Pt, and Ag).[209,210] Mercury-modified nanotubes have also been prepared, but the mercury was introduced as a salt solution.[211]

A few one-step procedures have also been developed. In one process the sample is allowed to react with an acidic gas mixture in elevated temperatures.[212] Carbon dust and transition metals are simultaneously removed during this treatment, which is relatively short, 10–30 min. Another process combines air treatment and acid microwave digestion to remove a high percentage of the metal and decreasing the purification operation time.[213] There have also been reports claiming that it is possible to selectively create surface oxygen groups on the inner nanotube wall, by HNO_3 oxidation.[214]

The reports on surface area change differ greatly. Some groups claim that the surface area and H_2 storage capacity increase considerably.[215,216] Other groups report the complete opposite result, due to material compaction.[199]

Compared to ball-milling, acidic boiling is more destructive. According to this particular study, the same quantity of —OH, —COOH, and —C═O were found after 20 min of ball-milling combined with 30 minutes of boiling in concentrated HNO_3, as for 100 minutes acidic boiling. However, only 3.5% of the ball-milled sample, while 18% of the long-term boiled samples was consumed.[171]

Fluorination

Fluorination is a common first step in the attempt to functionalize SWNTs and MWNTs. The nanotube is reacted with F_2 gas and thereafter some of the F substituents can be exchanged by nucleophilic substitution, leading to side-wall functionalization. After the reaction the remaining F can be partially or completely eliminated.[217] Hydrazine[218] and $LiBH_4/LiAlH_4$ can be used for defluorination of tubes.[219] Preferred nucleophiles include alkyl lithium species.[217] It has been established that the electrical properties of MWNTs change after fluorination, leading to a wide range of electrical structures, from insulating over to semiconducting and metallic-like behavior.[220–222]

Other Treatments

It is possible to attach different types of functional groups to the individual SWNT by applying a potential field,[223] so called nanolithography or electrochemistry. Furthermore, it is also possible to control the thickness of the deposit layer by varying the treatment duration. It is assumed that the reaction takes place primarily on defect sites on the tubes.

Multiwalled carbon nanotubes, SWNTs, and graphite can also be functionalized using hydrogen. The highest H content reached was about C_8H, which introduces a disturbance in the graphitic structures.[224] A way to functionalize the tubes without creating covalent bonds is to immobilize molecules on the nanotube surface by π–π-interaction.[225] In this way the structure of the nanotube is not disturbed, and the electrical properties are kept intact. Nanotubes have also been modified in order to investigate bio-systems, such as the adsorption behavior of proteins, taking place on a functionalized side-wall. For example, SWNTs have also been modified by co-

functionalization of protein-resistant polymers and biotin, creating a specific binding of streptavidin onto the SWNT.[226] Amino-dextran and periodate-oxidized dextran chains have also been immobilized onto plasma treated nanotubes. The resulting poly-saccharide grafted nanotubes are very hydrophobic.[227]

Using Surfactants

The role of a surfactant is to produce an efficient coating and induce electrostatic or steric repulsions that could counterbalance van der Waals attractions.[228] In our case, the electrostatic repulsion provided by adsorbed surfactants stabilizes the nanotubes against the strong van der Waals interaction between the tubes, hence preventing agglomeration. Polymer coated objects experience a reversible force. The polymer adsorbs onto the nanotube and repulsive forces dominate over attractive van der Waals forces between the carbon nanotubes. This balance of repulsive and attractive forces creates a thermodynamically stable dispersion, which might even result in separation of SWNTs from the bundles into individual nanotubes.

Surfactants have been used to disperse carbon nanotubes in several cases.[229–232] Some examples of commonly used surfactants are sodium dodecyl sulfate (SDS), both for SWNTs[233–235] and MWNTs,[236,237] and Triton X-100 (TX-100)[235,236,238] for SWNTs. Single-walled carbon nanotubes have also been dispersed using lithium dodecyl sulfate (LDS) as surfactant.[239,240]

In contrast, poly(vinyl alcohol) (PVA) is not efficient at stabilizing the tubes.[234] It has also been reported that neither negatively charged SDS, positively charged cetyltrimethyl ammonium chloride (CTAC) and dodecyltrimethyl ammonium bromide (DTAB), nonionic pentaoxoethylenedodecyl ether ($C_{12}E_5$), polysaccharide (Dextrin), nor long chain synthetic polymer poly(ethylene oxide) (PEO) could act as efficient dispersing agents for SWNTs in aqueous solutions.[241] However, Gum Arabic (GA) is reported to be an excellent stabilizer for SWNTs in water. Both SDS[242–244] and TX-100[245–248] have previously been used as surfactants for carbon black. A problem with surfactant induced dispersions is finding a feasible way to remove the surfactant from the final product.[249]

In-Situ Production of NTs

One way to solve the dispersion problem is to try to produce the carbon nanotube directly into the matrix, so called in-situ production. Attempts have been made to produce MWNT in several different Me–Al_2O_3 composites, where Me can be Fe, Co, Ni, or their alloys. The production step was followed by hot-pressing. Both MWNT and SWNT were found in the composite. However, the composites showed no improvement in physical properties.[250–252] As mentioned earlier, carbon nanotubes have been hot-pressed in MeO, and it was observed that the tubes were destroyed when the temperature in the hot-press was kept above 1200°C, resulting in the absence of property improvements.[134]

Production Technical Solutions

SiO_2 glass rods of micrometer sizes ($l = 10$–$15\,\mu m$, $d = 0.5$–$1.5\,\mu m$), containing 6 wt.% nanotubes, were prepared by using a surfactant (C_{16}TMAB). The micro-rods were incorporated in SiO_2 tablets with a loading of 60 wt.%, to promote nanotube dispersion in the tablet. The Vicker's hardness increased in both cases, but the effect was larger for micro-rods with nanotubes (~100% increase) than for rods without. It was observed that the micro-rods were not broken at the tablet fracture surface.[253]

Electrical Mechanisms

It is possible to break carbon nanotubes by applying an applied electrical field externally. The CNTs can then emit electrons and if the applied voltage exceeds the binding energy of a carbon atom, the atoms can be split off the tip. As a result, external graphite layers get broken and may peel off.[95]

Open-ended NTs placed close to each other can even rebond to form conducting electrical contacts.[84] Bending, defects, tube–tube contacts strongly modify the electrical behavior of NT. Structural topological defects always increase the resistance of metallic NTs to an extent that is strongly dependent on the defect density per unit length. Fusion has also been observed in other cases, not involving electrical fields. In one investigation MWNTs were extended 2–12% length-wise before failure. The breakage creates two open tube-ends, but they fuse together internally in a matter of tenths of seconds, resulting in two new, closed tubes.[254]

CONCLUSION

Dispersing carbon nanotubes into liquids can be achieved through either mechanical (physical) or chemical methods, which can be a very challenging task depending on the quality and surface morphology of the nanotubes used.

ACKNOWLEDGMENTS

The authors would like to acknowledge Rodney Andrews and David Jacques of the Center for Applied Energy Research for supplying the MWNTs, and Alan Dozier of the Electron Microscopy Center for providing TEM photomicrographs of the nanotubes.

REFERENCES

1. Kumar, V.; Chandra, Y. Characterization of epoxy resin system and dispersion of carbon black powder. J. Polym. Mater. **1989**, *6* (1), 51–56.
2. Shu, D.J.; Gong, X.G. Curvature effect on surface diffusion: The nanotube. J. Chem. Phys. **2001**, *114* (24), 10922–10926.
3. Kleiner, A.; Eggert, S. Curvature, hybridization, and STM images of carbon nanotubes. Phys. Rev. B **2001**, *64* (11), 113402/1–113402/4.
4. Hilding, J.; Grulke, E.A.; Sinnott, S.B.; Qian, D.; Andrews, R.; Jagtoyen, M. Sorption of butane on carbon multiwall nanotubes at room temperature. Langmuir **2001**, *17* (24), 7540–7544.
5. Stephan, O.; Ajayan, P.M.; Colliex, C.; Cyrot-Lackmann, F.; Sandre, E. Curvature-induced bonding changes in carbon nanotubes investigated by electron energy-loss spectrometry. Phys. Rev. B **1996**, *53* (20), 13824–13829.
6. Reed, B.W.; Sarikaya, M.; Dalton, L.R.; Bertsch, G.F. Transmission electron energy-loss spectroscopy study of carbon nanotubes upon high temperature treatment. Appl. Phys. Lett. **2001**, *78* (21), 3358–3360.
7. Botton, G.A.; Burnell, G.; Humphreys, C.J.; Yadav, T.; Withers, J.C. Microstructural and electron spectroscopic characterization of carbon nanostructures and nanotubes produced using multimetal catalysts. J. Phys. Chem. Solids **1997**, *58* (7), 1091–1102.
8. Knupfer, M.; Pichler, T.; Golden, M.S.; Fink, J.; Rinzler, A.; Smalley, R.E. Electron energy-loss spectroscopy studies of single wall carbon nanotubes. Carbon **1999**, *37* (5), 733–738.
9. Stephan, O.; Kociak, M.; Henrard, L.; Suenaga, K.; Gloter, A.; Tence, M.; Sandre, E.; Colliex, C. Electron energy-loss spectroscopy on individual nanotubes. J. Electron Spectrosc. **2001**, *114–116*, 209–217.
10. Yase, K.; Horiuchi, S.; Kyotani, M.; Yumura, M.; Uchida, K.; Ohshima, S.; Kuriki, Y.; Ikazaki, F.; Yamahira, N. Angular-resolved EELS of a carbon nanotube. Thin Solid Films **1996**, *273* (1–2), 222–224.
11. Guo, T.; Nikolaev, P.; Rinzler, A.G.; Tomanek, D.; Colbert, D.T.; Smalley, R.E. Self-assembly of tubular fullerenes. J. Phys. Chem. **1995**, *99* (27), 10694–10697.
12. Guo, T.; Nikolaev, P.; Thess, A.; Colbert, D.T.; Smalley, R.E. Catalytic growth of single-walled nanotubes by laser vaporization. Chem. Phys. Lett. **1995**, *243* (1,2), 49–54.
13. Yudasaka, M.; Komatsu, T.; Ichihashi, T.; Iijima, S. Single-wall carbon nanotube formation by laser ablation using double-targets of carbon and metal. Chem. Phys. Lett. **1997**, *278* (1,2,3), 102–106.
14. Thess, A.; Lee, R.; Nikolaev, P.; Dai, H.; Petit, P.; Robert, J.; Xu, C.; Lee, Y.H.; Kim, S.G. et al. Crystalline ropes of metallic carbon nanotubes. Science (Washington, D. C.) **1996**, *273* (5274), 483–487.
15. Sun, L.F.; Mao, J.M.; Pan, Z.W.; Chang, B.H.; Zhou, W.Y.; Wang, G.; Qian, L.X.; Xie, S.S. Growth of straight nanotubes with a cobalt-nickel catalyst by chemical vapor deposition. Appl. Phys. Lett. **1999**, *74* (5), 644–646.
16. Yudasaka, M.; Sensui, N.; Takizawa, M.; Bandow, S.; Ichihashi, T.; Iijima, S. Formation of single-wall carbon nanotubes catalyzed by Ni separating from Y in laser ablation or in arc discharge using a C target containing a NiY catalyst. Chem. Phys. Lett. **1999**, *312* (2–4), 155–160.
17. Yudasaka, M.; Yamada, R.; Sensui, N.; Wilkins, T.; Ichihashi, T.; Iijima, S. Mechanism of the effect of NiCo, Ni and Co catalysts on the yield of single-wall carbon nanotubes formed by pulsed Nd : YAG laser ablation. J. Phys. Chem. B **1999**, *103* (30), 6224–6229.
18. Hernandez, E.; Ordejon, P.; Boustani, I.; Rubio, A.; Alonso, J.A. Tight binding molecular dynamics studies of boron assisted nanotube growth. J. Chem. Phys. **2000**, *113* (9), 3814–3821.
19. Blase, X.; Charlier, J.C.; De Vita, A.; Car, R.; Redlich, P.; Terrones, M.; Hsu, W.K.; Terrones, H.; Carroll, D.L.; Ajayan, P.M. Boron-mediated growth of long helicity-selected carbon nanotubes. Phys. Rev. Lett. **1999**, *83* (24), 5078–5081.
20. Yudasaka, M.; Zhang, M.; Iijima, S. Porous target enhances production of single-wall carbon nanotubes by laser ablation. Chem. Phys. Lett. **2000**, *323* (5,6), 549–553.
21. Laplaze, D.; Bernier, P.; Barbedette, L.; Lambert, J.M.; Flamant, G.; Lebrun, M.; Brunelle, A.; Della-Negra, S. Production of fullerenes from solar energy: The Odeillo experiment.

C. R. Acad. Sci., Ser. II: Mec., Phys., Chim., Astron. **1994**, *318* (6), 733–738.
22. Chibante, L.P.F.; Thess, A.; Alford, J.M.; Diener, M.D.; Smalley, R.E. Solar generation of the fullerenes. J. Phys. Chem. **1993**, *97* (34), 8696–8700.
23. Fields, C.L.; Pitts, J.R.; Hale, M.J.; Bingham, C.; Lewandowski, A.; King, D.E. Formation of fullerenes in highly concentrated solar flux. J. Phys. Chem. **1993**, *97* (34), 8701–8702.
24. Bernier, P.; Laplaze, D.; Auriol, J.; Barbedette, L.; Flamant, G.; Lebrun, M.; Brunelle, A.; Della-Negra, S. Production of fullerenes from solar energy. Synth. Met. **1995**, *70* (1–3), 1455–1456.
25. Laplaze, D.; Bernier, P.; Journet, C.; Vie, V.; Flamant, G.; Lebrun, M. Carbon sublimation using a solar furnace. Synthetic Met. **1997**, *86* (1–3), 2295–2296.
26. Laplaze, D.; Bernier, P.; Journet, C.; Sauvajol, J.L.; Bormann, D.; Flamant, G.; Lebrun, M. The use of solar energy for the production of fullerenes and porous silicon. J. Phys. III **1997**, *7* (3), 463–472.
27. Laplaze, D.; Bernier, P.; Flamant, G.; Lebrun, M.; Brunelle, A.; Della-Negra, S. Preparation of fullerenes using a solar furnace. Synth. Met. **1996**, *77* (1–3), 67–71.
28. Heben, M.J.; Bekkedahl, T.A.; Schultz, D.L.; Jones, K.M.; Dillon, A.C.; Curtis, C.J.; Bingham, C.; Pitts, J.R.; Lewandowski, A.; Fields C.L. In *Proceedings of the Symposium on Recent Advances in the Chemistry and Physics of Fullerenes and Related Materials*, 1996; The Electrochemical Society Inc.
29. Laplaze, D.; Bernies, J.; Journet, C.P.; Vie, V.; Flamant, G.; Philippot, E.; Lebrun, M. In *Proceedings of the 8th International Symposium on Solar Thermal Concentrating Technologies*, Köln, Germany, 1996.
30. Fields, C.L.P., J.R.; Mischler, D.; Bingham, C.; Lewandowski, A.; Schultz, D.L.; Bekkedahl, T.A.; Jones, K.M.; Heben, M.J. In *Proceedings of the 8th International Symposium on Solar Thermal Concentrating Technologies*, Köln, Germany, 1996.
31. Laplaze, D.; Bernier, P.; Maser, W.K.; Flamant, G.; Guillard, T.; Loiseau, A. Carbon nanotubes: the solar approach. Carbon **1998**, *36* (5–6), 685–688.
32. Iijima, S. Helical microtubules of graphitic carbon. Nature (London), **1991**, *354* (6348), 56–58.
33. Ebbesen, T.W.; Ajayan, P.M. Large-scale synthesis of carbon nanotubes. Nature (London), **1992**, *358* (6383), 220–222.
34. Ebbesen, T.W.; Carbon nanotubes. Annu. Rev. Mater. Sci. **1994**, *24*, 235–264.
35. Loiseau, A.; Pascard, H. Synthesis of long carbon nanotubes filled with Se, S, Sb and Ge by the arc method. Chem. Phys. Lett. **1996**, *256* (3), 246–252.
36. Guerret-Piecourt, C.; Le Bouar, Y.; Loiseau, A.; Pascard, H. Relation between metal electronic structure and morphology of metal compounds inside carbon nanotubes. Nature (London) **1994**, *372* (6508), 761–765.
37. Ata, M.; Hudson, A.J.; Yamura, K.; Kurihara, K.I. Carbon nanotubes filled with gadolinium and hafnium carbides. Jpn. J. Appl. Phys., Part 1 **1995**, *34* (8A), 4207–4212.
38. Lin, X.; Wang, X.K.; Dravid, V.P.; Chang, R.P.H.; Ketterson, J.B.; Large scale synthesis of single-shell carbon nanotubes. Appl. Phys. Lett. **1994**, *64* (2), 181–183.
39. Ajayan, P.M.; Colliex, C.; Lambert, J.M.; Bernier, P.; Barbedette, L.; Tence, M.; Stephan, O. Growth of manganese filled carbon nanofibers in the vapor phase. Phys. Rev. Lett. **1994**, *72* (11), 1722–1725.
40. Seraphin, S.; Zhou, D.; Jiao, J.; Minke, M.A.; Wang, S.; Yadav, T.; Withers, J.C. Catalytic role of nickel, palladium, and platinum in the formation of carbon nanoclusters. Chem. Phys. Lett. **1994**, *217* (3), 191–198.
41. Saito, Y.; Kawabata, K.; Okuda, M. Single-layered carbon nanotubes synthesized by catalytic assistance of rare-earths in a carbon arc. J. Phys. Chem. **1995**, *99* (43), 16076–16079.
42. Kim, M.S.; Rodriguez, N.M.; Baker, R.T.K. Interaction of hydrocarbons with copper-nickel and nickel in the formation of carbon filaments. J. Catal. **1991**, *131* (1), 60–73.
43. Kiang, C.-H.; Goddard, W.A., III; Beyers, R.; Salem, J.R.; Bethune, D.S. Catalytic synthesis of single-layer carbon nanotubes with a wide range of diameters. J. Phys. Chem. **1994**, *98* (26), 6612–6618.
44. Subramoney, S.R., Ruoff, R.S.; Lorents, D.C.; Malhotra, R. Radial single-layer nanotubes. Nature **1993**, *366* (637).
45. Journet, C.; Maser, W.K.; Bernier, P.; Loiseau, A.; Lamy de la Chapells, M.; Lefrant, S.; Deniard, P.; Lee, R.; Fischer, J.E. Large-scale production of single-walled carbon nanotubes by the electric-arc technique. Nature (London), **1997**, *388* (6644), 756–758.
46. Takizawa, M.; Bandow, S.; Torii, T.; Iijima, S. Effect of environment temperature for synthesizing single-

wall carbon nanotubes by arc vaporization method. Chem. Phys. Lett. **1999**, *302* (1,2), 146–150.
47. Takizawa, M.; Bandow, S.; Yudasaka, M.; Ando, Y.; Shimoyama, H.; Iijima, S. Change of tube diameter distribution of single-wall carbon nanotubes induced by changing the bimetallic ratio of Ni and Y catalysts. Chem. Phys. Lett. **2000**, *326* (3,4), 351–357.
48. Kiang, C.-H.; Goddard, W.A., III; Beyers, R.; Salem, J.R.; Bethune, D.S. Catalytic effects of heavy metals on the growth of carbon nanotubes and nanoparticles. J. Phys. Chem. Solids **1996**, *57* (1), 35–39.
49. Setlur, A.A.; Lauerhaas, J.M.; Dai, J.Y.; Chang, R.P.H. A method for synthesizing large quantities of carbon nanotubes and encapsulated copper nanowires. Appl. Phys. Lett. **1996**, *69* (3), 345–347.
50. Yamashita, J.; Hirayama, H.; Ohshima, Y.; Takayanagi, K. Growth of a single-wall carbon nanotube in the gap of scanning tunneling microscope. Appl. Phys. Lett. **1999**, *74* (17), 2450–2452.
51. Bethune, D.S. Adding metal to carbon: Production and properties of metallofullerenes and single-layer nanotubes. NATO ASI Ser., Ser. E **1996**, *316* (Chemical Physics of Fullerenes 10 (and 5) Years Later), 165–181.
52. Kiang, C.-H.; Goddard, W.A., III. Polyyne ring nucleus growth model for single-layer carbon nanotubes. Phys. Rev. Lett. **1996**, *76* (14), 2515–2518.
53. Wang, X.K.; Lin, X.W.; Dravid, V.P.; Ketterson, J.B.; Chang, R.P.H. Carbon nanotubes synthesized in a hydrogen arc discharge. Appl. Phys. Lett. **1995**, *66* (18), 2430–2432.
54. Cadek, M.; Murphy, R.; McCarthy, B.; Drury, A.; Lahr, B.; Barklie, R.C.; in het Panhuis, M.; Coleman, J.N.; Blau, W.J. Optimization of the arc-discharge production of multi-walled carbon nanotubes. Carbon **2002**, *40* (6), 923–928.
55. Shi, Z.; Lian, Y.; Zhou, X.; Gu, Z.; Zhang, Y.; Iijima, S.; Zhou, L.; Yue, K.T.; Zhang, S. Mass-production of single-wall carbon nanotubes by arc discharge method. Carbon **1999**, *37* (9), 1449–1453.
56. Hsu, W.K.; Hare, J.P.; Terrones, M.; Kroto, H.W.; Walton, D.R.M.; Harris, P.J.F. Condensed-phase nanotubes. Nature (London) **1995**, *377* (6551), 687.
57. Hsu, W.K.; Terrones, M.; Hare, J.P.; Terrones, H.; Kroto, H.W.; Walton, D.R.M. Electrolytic formation of carbon nanostructures. Chem. Phys. Lett. **1996**, *262* (1,2), 161–166.
58. Pan, Z.W.; Xie, S.S.; Chang, B.H.; Wang, C.Y.; Lu, L.; Liu, W.; Zhou, W.Y.; Li, W.Z.; Qian, L.X. Very long carbon nanotubes. Nature (London) **1998**, *394* (6694), 631–632.
59. Andrews, R.; Jacques, D.; Rao, A.M.; Derbyshire, F.; Qian, D.; Fan, X.; Dickey, E.C.; Chen, J. Continuous production of aligned carbon nanotubes: A step closer to commercial realization. Chem. Phys. Lett. **1999**, *303* (5,6), 467–474.
60. Gao, R.; Wang, Z.L.; Fan, S. Kinetically controlled growth of helical and zigzag shapes of carbon nanotubes. J. Phys. Chem. B **2000**, *104* (6), 1227–1234.
61. Grobert, N.; Terrones, M.; Trasobares, S.; Kordatos, K.; Terrones, H.; Olivares, J.; Zhang, J.P.; Redlich, P.; Hsu, W.K.; Reeves, C.L.; Wallis, D.J.; Zhu, Y.Q.; Hare, J.P.; Pidduck, A.J.; Kroto, H.W.; Walton, D.R.M. A novel route to aligned nanotubes and nanofibers using laser-patterned catalytic substrates. Appl. Phys. A- Mater. **2000**, *70* (2), 175–183.
62. Kamalakaran, R.; Terrones, M.; Seeger, T.; Kohler-Redlich, P.; Ruhle, M.; Kim, Y.A.; Hayashi, T.; Endo, M. Synthesis of thick and crystalline nanotube arrays by spray pyrolysis. Appl. Phys. Lett. **2000**, *77* (21), 3385–3387.
63. Mayne, M.; Grobert, N.; Terrones, M.; Kamalakaran, R.; Ruhle, M.; Kroto, H.W.; Walton, D.R.M. Pyrolytic production of aligned carbon nanotubes from homogeneously dispersed benzene-based aerosols. Chem. Phys. Lett. **2001**, *338* (2,3), 101–107.
64. Cassell, A.M.; Verma, S.; Delzeit, L.; Meyyappan, M.; Han, J. Combinatorial optimization of heterogeneous catalysts used in the growth of carbon nanotubes. Langmuir **2001**, *17* (2), 260–264.
65. Cui, S.; Lu, C.Z.; Qiao, Y.L.; Cui, L. Large-scale preparation of carbon nanotubes by nickel catalyzed decomposition of methane at 600°C. Carbon **1999**, *37* (12), 2070–2073.
66. Willems, I.; Konya, Z.; Colomer, J.F.; Van Tendeloo, G.; Nagaraju, N.; Fonseca, A.; Nagy, J.B. Control of the outer diameter of thin carbon nanotubes synthesized by catalytic decomposition of hydrocarbons. Chem. Phys. Lett. **2000**, *317* (1,2), 71–76.
67. Iwasaki, T.; Motoi, T.; Den, T. Multiwalled carbon nanotubes growth in anodic alumina nanoholes. Appl. Phys. Lett. **1999**, *75* (14), 2044–2046.
68. Lee, C.J.; Park, J.; Kim, J.M.; Huh, Y.; Lee, J.Y.; No, K.S. Low-temperature growth of carbon nanotubes by thermal chemical vapor deposition using Pd, Cr, and Pt as co-catalyst. Chem. Phys. Lett. **2000**, *327* (5,6), 277–283.

69. Lee, C.J.; Park, J.H.; Park, J. Synthesis of bamboo-shaped multiwalled carbon nanotubes using thermal chemical vapor deposition. Chem. Phys. Lett. **2000**, *323* (5,6), 560–565.
70. Nath, M.; Satishkumar, B.C.; Govindaraj, A.; Vinod, C.P.; Rao, C.N.R. Production of bundles of aligned carbon and carbon-nitrogen nanotubes by the pyrolysis of precursors on silica-supported iron and cobalt catalysts. Chem. Phys. Lett. **2000**, *322* (5), 333–340.
71. Cassell, A.M.; Raymakers, J.A.; Kong, J.; Dai, H. Large scale CVD synthesis of single-walled carbon nanotubes. J. Phys. Chem. B **1999**, *103* (31), 6484–6492.
72. Franklin, N.R.; Dai, H. An enhanced CVD approach to extensive nanotube networks with directionality. Adv. Mater. (Weinheim, Germany) **2000**, *12* (12), 890–894.
73. Hafner, J.H.; Bronikowski, M.J.; Azamian, B.R.; Nikolaev, P.; Rinzler, A.G.; Colbert, D.T.; Smith, K.A.; Smalley, R.E. Catalytic growth of single-wall carbon nanotubes from metal particles. Chem. Phys. Lett. **1998**, *296* (1,2), 195–202.
74. Katoh, R.; Tasaka, Y.; Sekreta, E.; Yumura, M.; Ikazaki, F.; Kakudate, Y.; Fujiwara, S. Sonochemical production of a carbon nanotube. Ultrason. Sonochem. **1999**, *6* (4), 185–187.
75. Li, Y.L.; Yu, Y.D.; Liang, Y. A novel method for synthesis of carbon nanotubes: Low temp. solid pyrolysis. J. Mater. Res. **1997**, *12* (7), 1678–1680.
76. Jeong, S.-H.; Lee, O.-J.; Lee, K.-H.; Oh, S.H.; Park, C.-G. Preparation of aligned carbon nanotubes with prescribed dimensions: template synthesis and sonication cutting approach. Chem. Mater. **2002**, *14* (4), 1859–1862.
77. Peigney, A.; Laurent, C.; Dobigeon, F.; Rousset, A. Carbon nanotubes grown in situ by a novel catalytic method. J. Mater. Res. **1997**, *12* (3), 613–615.
78. Hulicova, D.; Hosoi, K.; Kuroda, S.-I.; Abe, H.; Oya, A. Carbon nanotubes prepared by spinning and carbonizing fine core-shell polymer microspheres. Adv. Mater. (Weinheim, Germany) **2002**, *14* (6), 452–455.
79. Cho, W.-S.; Hamada, E.; Kondo, Y.; Takayanagi, K. Synthesis of carbon nanotubes from bulk polymer. Appl. Phys. Lett. **1996**, *69* (2), 278–279.
80. Collins, P.G.; Hersam, M.; Arnold, M.; Martel, R.; Avouris, P. Current saturation and electrical breakdown in multiwalled carbon nanotubes. Phys. Rev. Lett. **2001**, *86* (14), 3128–3131.
81. Popov, M.; Kyotani, M.; Nemanich, R.J.; Koga, Y. Superhard phase composed of single-wall carbon nanotubes. Phys. Rev. B **2002**, *65* (3), 033408/1–033408/4.
82. Garg, A.; Sinnott, S.B. Effect of chemical functionalization on the mechanical properties of carbon nanotubes. Chem. Phys. Lett. **1998**, *295* (4), 273–278.
83. Ozaki, T.; Iwasa, Y.; Mitani, T. Stiffness of single-walled carbon nanotubes under large strain. Phys. Rev. Lett. **2000**, *84* (8), 1712–1715.
84. Buongiorno Nardelli, M.; Fattebert, J.L.; Orlikowski, D.; Roland, C.; Zhao, Q.; Bernholc, J. Mechanical properties, defects and electronic behavior of carbon nanotubes. Carbon **2000**, *38* (11–12), 1703–1711.
85. Tekleab, D.; Carroll, D.L.; Samsonidze, G.G.; Yakobson, B.I. Strain-induced electronic property heterogeneity of a carbon nanotube. Phys. Rev. B **2001**, *64* (3), 035419/1–035419/5.
86. Rochefort, A.; Avouris, P.; Lesage, F.; Salahub, D.R. Electrical and mechanical properties of distorted carbon nanotubes. Phys. Rev. B **1999**, *60* (19), 13824–13830.
87. Bernholc, J.; Brabec, C.; Nardelli, M.B.; Maiti, A.; Roland, C.; Yakobson, B.I. Theory of growth and mechanical properties of nanotubes. Appl. Phys. A- Mater. **1998**, *A67* (1), 39–46.
88. Muster, J.; Burghard, M.; Roth, S.; Duesberg, G.S.; Hernandez, E.; Rubio, A. Scanning force microscopy characterization of individual carbon nanotubes on electrode arrays. J. Vac. Sci. Technol. B **1998**, *16* (5), 2796–2801.
89. Yu, M.-F.; Lourie, O.; Dyer, M.J.; Moloni, K.; Kelly, T.F.; Ruoff, R.S. Strength and breaking mechanism of multiwalled carbon nanotubes under tensile load. Science (Washington, D. C.) **2000**, *287* (5453), 637–640.
90. Salvetat, J.P.; Bonard, J.M.; Thomson, N.H.; Kulik, A.J.; Forro, L.; Benoit, W.; Zuppiroli, L. Mechanical properties of carbon nanotubes. Appl. Phys. A- Mater. **1999**, *69* (3), 255–260.
91. Xie, S.; Li, W.; Pan, Z.; Chang, B.; Sun, L. Mechanical and physical properties on carbon nanotube. J. Phys. Chem. Solids **2000**, *61* (7), 1153–1158.
92. Treacy, M.M.J.; Ebbesen, T.W.; Gibson, J.M. Exceptionally high Young's modulus observed for individual carbon nanotubes. Nature (London), **1996**, *381* (6584), 678–680.
93. Wong, E.W.; Sheehan, P.E.; Lieber, C.M. Nanobeam mechanics: Elasticity, strength, and toughness of nanorods and nanotubes. Science (Washington, D. C.) **1997**, *277* (5334), 1971–1975.

94. Shen, W.; Jiang, B.; Han, B.S.; Xie, S.-S. Investigation of the radial compression of carbon nanotubes with a scanning probe microscope. Phys. Rev. Lett. **2000**, *84* (16), 3634–3637.
95. Wang, Z.L.; Gao, R.P.; Poncharal, P.; de Heer, W.A.; Dai, Z.R.; Pan, Z.W. Mechanical and electrostatic properties of carbon nanotubes and nanowires. Mat. Sci. Eng. C-Bio. S **2001**, *C16* (1–2), 3–10.
96. Salvetat, J.-P.; Briggs, G.A.D.; Bonard, J.-M.; Bacsa, R.R.; Kulik, A.J.; Stockli, T.; Burnham, N.A.; Forro, L. Elastic and shear moduli of single-walled carbon nanotube ropes. Phys. Rev. Lett. **1999**, *82* (5), 944–947.
97. Yu, M.-F.; Files, B.S.; Arepalli, S.; Ruoff, R.S. Tensile loading of ropes of single wall carbon nanotubes and their mechanical properties. Phys. Rev. Lett. **2000**, *84* (24), 5552–5555.
98. Krishnan, A.; Dujardin, E.; Ebbesen, T.W.; Yianilos, P.N.; Treacy, M.M.J. Young's modulus of single-walled nanotubes. Phys. Rev. B **1998**, *58* (20), 14013–14019.
99. Zhou, G.; Duan, W.; Gu, B. First-principles study on morphology and mechanical properties of single-walled carbon nanotube. Chem. Phys. Lett. **2001**, *333* (5), 344–349.
100. Popov, V.N.; Van Doren, V.E.; Balkanski, M. Elastic properties of single-walled carbon nanotubes. Phys. Rev. B **2000**, *61* (4), 3078–3084.
101. Gao, G.; Cagin, T.; Goddard, W.A., III. Energetics, structure, mechanical and vibrational properties of single-walled carbon nanotubes. Nanotechnology, **1998**, *9* (3), 184–191.
102. Lu, J.P. Elastic properties of carbon nanotubes and nanoropes. Phys. Rev. Lett. **1997**, *79* (7), 1297–1300.
103. Yao, Z.; Zhu, C.-C.; Cheng, M.; Liu, J. Mechanical properties of carbon nanotube by molecular dynamics simulation. Comp. Mater. Sci. **2001**, *22* (3–4), 180–184.
104. Goze, C.; Vaccarini, L.; Henrard, L.; Bernier, P.; Hernandez, E.; Rubio, A. Elastic and mechanical properties of carbon nanotubes. Synthetic Met. **1999**, *103* (1–3), 2500–2501.
105. Dresselhaus, M.S.E.A., *Graphite Fibers and Filaments*; Springer-Verlag: New York, 1988.
106. Peebles, L.H., Jr. *Carbon Fibers: Formation, Structure, and Properties;* CRC Press: Boca Raton, FL, 1995; 224 pp.
107. Jacobsen, R.L.; Tritt, T.M.; Guth, J.R.; Ehrlich, A.C.; Gillespie, D.J. Mechanical properties of vapor-grown carbon fiber. Carbon **1995**, *33* (9), 1217–1221.
108. Kelly, B.T. *Physics of Graphite;* Appl. Sci. Publ. Ltd.: Barking, England, 1981; 475 pp.
109. Blakslee, O.L.; Proctor, D.G.; Seldin, E.J.; Spence, G.B. Elastic constants of compression-annealed pyrolytic graphite. J. Appl. Phys. **1970**, *41* (8), 3373–3382.
110. Overney, G.; Zhong, W.; Tomanek, D. Structural rigidity and low frequency vibrational modes of long carbon tubules. Z. Phys. D: At. Mol. Clusters **1993**, *27* (1), 93–96.
111. Pierson, H.O. *Handbook of Carbon, Graphite, Diamond, and Fullerenes: Properties, Processing, and Applications*; Noyes Publications: Park Ridge, NJ, 1993.
112. Tibbetts, G.G.; Beetz, C.P., Jr. Mechanical properties of vapor-grown carbon fibers. J. Phys. D: Appl. Phys. **1987**, *20* (3), 292–297.
113. Thostenson, E.T.; Ren, Z.; Chou, T.W. Advances in the science and technology of carbon nanotubes and their composites: a review. Compos. Sci. Technol. **2001**, *61* (13), 1899–1912.
114. Endo, M.; Kim, Y.A.; Matusita, T.; Hayashi, T. From vapor-grown carbon fibers (VGCFs) to carbon nanotubes. NATO Science Series, Series E: Applied Sciences **2001**, *372* (Carbon Filaments and Nanotubes: Common Origins, Differing Applications?), 51–61.
115. Hone, J.; Whitney, M.; Piskoti, C.; Zettl, A. Thermal conductivity of single-walled carbon nanotubes. Phys. Rev. B **1999**, *59* (4), R2514–R2516.
116. Hone, J.; Llaguno, M.C.; Nemes, N.M.; Johnson, A.T.; Fischer, J.E.; Walters, D.A.; Casavant, M.J.; Schmidt, J.; Smalley, R.E. Electrical and thermal transport properties of magnetically aligned single wall carbon nanotube films. Appl. Phys. Lett. **2000**, *77* (5), 666–668.
117. Che, J.; Cagin, T.; Goddard, W.A., III. Thermal conductivity of carbon nanotubes. Nanotechnology **2000**, *11* (2), 65–69.
118. Radosavljevic, M.; Lefebvre, J.; Johnson, A.T. High-field electrical transport and breakdown in bundles of single-wall carbon nanotubes. Phys. Rev. B **2001**, *64* (24), 241307/1–241307/4.
119. Reulet, B.; Kasumov, A.Y.; Kociak, M.; Deblock, R.; Khodos, I.I.; Gorbatov, Y.B.; Volkov, V.T.; Journet, C.; Bouchiat, H. Acoustoelectric Effects in Carbon Nanotubes. Phys. Rev. Lett. **2000**, *85* (13), 2829–2832.
120. Kim, P.; Shi, L.; Majumdar, A.; McEuen, P.L. Thermal transport measurements of individual multiwalled nanotubes. Phys. Rev. Lett. **2001**, *87* (21), 215502/1–215502/4.
121. Berber, S.; Kwon, Y.-K.; Tomanek, D. Unusually high thermal conductivity of carbon nanotubes. Phys. Rev. Lett. **2000**, *84* (20), 4613–4616.

122. Kaneto, K.; Tsuruta, M.; Sakai, G.; Cho, W.Y.; Ando, Y. Electrical conductivities of multi-wall carbon nanotubes. Synthetic Met. **1999**, *103* (1–3), 2543–2546.
123. Zettl, A.; Cumings, J. Electromechanical properties of multiwall carbon nanotubes. AIP Conf. Proc. **2001**, *590* (Nanonetwork Materials), 107–112.
124. Weast, R.C.; Astle, M.J.; Boyer, W.H., Eds.; *CRC Handbook of Chemistry and Physics.*, 67th Ed.; CRC Press, Inc.: Boca, Raton, FL, 1986.
125. http://www.zyvex.com/nanotech/talks/XeroxPARC980312/sld034.htm (accessed Aug 2002).
126. Biercuk, M.J.; Llaguno, M.C.; Radosavljevic, M.; Hyun, J.K.; Johnson, A.T.; Fischer, J.E. Carbon nanotube composites for thermal management. Los Alamos National Laboratory, Preprint Archive, Condensed Matter **2002**, 1–12, arXiv:cond-mat/0205418.
127. Sandler, J.; Shaffer, M.S.P.; Prasse, T.; Bauhofer, W.; Schulte, K.; Windle, A.H. Development of a dispersion process for carbon nanotubes in an epoxy matrix and the resulting electrical properties. Polymer **1999**, *40* (21), 5967–5971.
128. Coleman, J.N.; Curran, S.; Dalton, A.B.; Davey, A.P.; Mc Carthy, B.; Blau, W.; Barklie, R.C. Physical doping of a conjugated polymer with carbon nanotubes. Synthetic Met. **1999**, *102* (1–3), 1174–1175.
129. Lozano, K.; Bonilla-Rios, J.; Barrera, E.V. A study on nanofiber-reinforced thermoplastic composites (II), investigation of the mixing rheology and conduction properties. J. Appl. Polym. Sci. **2001**, *80* (8), 1162–1172.
130. Garza, R.L., K.; Guerrero, C. *Mmemorias de Compositos 1993*, Saltillo Coahuila: Mexico, 1993.
131. Dutta, A.L.; Misra, A.K.; Singh, R.P. Electrical conduction and ultrasound wave propagation in particulate and short fiber composites of PVC. II: PVC-aluminum coated glass fiber composites. J. Vinyl Technol. **1992**, *14* (2), 93–100.
132. Curran, S.A.; Ajayan, P.M.; Blau, W.J.; Carroll, D.L.; Coleman, J.N.; Dalton, A.B.; Davey, A.P.; Drury, A.; McCarthy, B.; Maier, S.; Strevens, A. A composite from poly(m-phenylenevinylene-co-2,5-dioctoxy-p-phenylenevinylene) and carbon nanotubes. A novel material for molecular optoelectronics. Adv. Mater. (Weinheim, Germany) **1998**, *10* (14), 1091–1093.
133. Andrews, R.; Jacques, D.; Rao, A.M.; Rantell, T.; Derbyshire, F.; Chen, Y.; Chen, J.; Haddon, R.C. Nanotube composite carbon fibers. Appl. Phys. Lett. **1999**, *75* (9), 1329–1331.
134. Flahaut, E.; Peigney, A.; Laurent, C.; Marliere, C.; Chastel, F.; Rousset, A. Carbon nanotube-metal-oxide nanocomposites: Microstructure, electrical conductivity and mechanical properties. Acta Mater. **2000**, *48* (14), 3803–3812.
135. Haggenmueller, R.; Gommans, H.H.; Rinzler, A.G.; Fischer, J.E.; Winey, K.I. Aligned single-wall carbon nanotubes in composites by melt processing methods. Chem. Phys. Lett. **2000**, *330* (3,4), 219–225.
136. Ito, F.; Konuma, K.; Okamoto, A. Electron emission from single-walled carbon nanotubes with sharpened bundles. J. Appl. Phys. **2001**, *89* (12), 8141–8145.
137. Schadler, L.S.; Giannaris, S.C.; Ajayan, P.M. Load transfer in carbon nanotube epoxy composites. Appl. Phys. Lett. **1998**, *73* (26), 3842–3844.
138. Qian, D.; Dickey, E.C.; Andrews, R.; Rantell, T. Load transfer and deformation mechanisms in carbon nanotube-polystyrene composites. Appl. Phys. Lett. **2000**, *76* (20), 2868–2870.
139. Gong, X.; Liu, J.; Baskaran, S.; Voise, R.D.; Young, J.S. Surfactant-assisted processing of carbon nanotube/polymer composites. Chem. Mater. **2000**, *12* (4), 1049–1052.
140. Jia, Z.; Wang, Z.; Xu, C.; Liang, J.; Wei, B.; Wu, D.; Zhu, S. Study on poly(methyl methacrylate)/carbon nanotube composites. Mat. Sci. Eng. A-Struct. **1999**, *A271* (1–2), 395–400.
141. Jin, Z.; Pramoda, K.P.; Xu, G.; Goh, S.H. Dynamic mechanical behavior of melt-processed multi-walled carbon nanotube/poly(methyl methacrylate) composites. Chem. Phys. Lett. **2001**, *337* (1,2,3), 43–47.
142. Jin, Z.; Pramoda, K.P.; Goh, S.H.; Xu, G. Poly(vinylidene fluoride)-assisted melt-blending of multi-walled carbon nanotube/poly(methyl methacrylate) composites. Mater. Res. Bull. **2002**, *37* (2), 271–278.
143. Baughman, R.H.; Cui, C.; Zakhidov, A.A.; Iqbal, Z.; Barisci, J.N.; Spinks, G.M.; Wallace, G.G.; Mazzoldi, A.; De Rossi, D.; Rinzler, A.G.; Jaschinski, O.; Roth, S.; Kertesz, M. Carbon nanotube actuators. Science (Washington, D. C.) **1999**, *284* (5418), 1340–1344.
144. Vigolo, B.; Penicaud, A.; Coulon, C.; Sauder, C.; Pailler, R.; Journet, C.; Bernier, P.; Poulin, P. Dispersions and fibers of carbon nanotubes. Materials Research Society Symposium Proceedings **2001**, *633* (Nanotubes and Related Materials), A12.1.1–A12.1.9.
145. Vigolo, B.; Penicaud, A.; Coulon, C.; Sauder, C.; Pailler, R.; Journet, C.; Bernier, P.; Poulin, P. Macroscopic fibers and ribbons of oriented carbon

nanotubes. Science (Washington, D. C.) **2000**, *290* (5495), 1331–1334.
146. Siegel, R.W.; Chang, S.K.; Ash, B.J.; Stone, J.; Ajayan, P.M.; Doremus, R.W.; Schadler, L.S. Mechanical behavior of polymer and ceramic matrix nanocomposites. Scripta Mater. **2001**, *44* (8/9), 2061–2064.
147. McCoy, B.J., Wang, M. Continuous mixture fragmentation kinetics: Particle size reduction and molecular cracking. Chem. Eng. Sci. **1994**, *49* (22), 3773.
148. Rangarajan, P.; Bhattacharyya, D.; Grulke, E.A. HDPE liquefaction: random chain scission model. J. Appl. Polym. Sci. **1998**, *70* (6), 1239–1251.
149. Wang, M.; Smith, J.M.; McCoy, B.J. Continuous mixture kinetics for thermal degradation of poly (styrene-allyl alcohol) in solution. AIChE J. **1995**, *41* (6), 1521.
150. Zhang, M.; Yudasaka, M.; Koshio, A.; Jabs, C.; Ichihashi, T.; Iijima, S. Structure of single-wall carbon nanotubes purified and cut using polymer. Appl. Phys. A-Mater. **2002**, *74* (1), 7–10.
151. Koshio, A.; Yudasaka, M.; Iijima, S. Thermal degradation of ragged single-wall carbon nanotubes produced by polymer-assisted ultrasonication. Chem. Phys. Lett. **2001**, *341* (5,6), 461–466.
152. Koshio, A.; Yudasaka, M.; Zhang, M.; Iijima, S. A simple way to chemically react single-wall carbon nanotubes with organic materials using ultrasonication. Nano Lett. **2001**, *1* (7), 361–363.
153. Esumi, K.; Ishigami, M.; Nakajima, A.; Sawada, K.; Honda, H. Chemical treatment of carbon nanotubes. Carbon **1996**, *34* (2), 279–281.
154. Shelimov, K.B.; Esenaliev, R.O.; Rinzler, A.G.; Huffman, C.B.; Smalley, R.E. Purification of single-wall carbon nanotubes by ultrasonically assisted filtration. Chem. Phys. Lett. **1998**, *282* (5,6), 429–434.
155. Yudasaka, M. Carbon nanotubes, environmentally benign new materials. Jidosha Gijutsukai Chubu Shibuho **2002**, *51*, 48–51.
156. Ausman, K.D.; O'Connell, M.J.; Boul, P.; Ericson, L.M.; Casavant, M.J.; Walters, D.A.; Huffman, C.; Saini, R.; Wang, Y.; Haroz, E.; Billups, E.W.; Smalley, R.E. Roping and wrapping carbon nanotubes. AIP Conf. Proc. **2001**, *591* (Electronic Properties of Molecular Nanostructures), 226–230.
157. Haluska, M.; Hulman, M.; Hirscher, M.; Becher, M.; Roth, S.; Stepanek, I.; Bernier, P. Hydrogen storage in mechanically treated single wall carbon nanotubes. AIP Conf. Proc. **2001**, *591* (Electronic Properties of Molecular Nanostructures), 603–608.
158. Lu, K.L.; Lago, R.M.; Chen, Y.K.; Green, M.L.H.; Harris, P.J.F.; Tsang, S.C. Mechanical damage of carbon nanotubes by ultrasound. Carbon **1996**, *34* (6), 814–816.
159. Povey, M.J.W., Mason, T.J. *Ultrasound in Food Processing*; Blackie Academic and Professional: Glasgow, Scotland, 1998.
160. Karicherla, A. Shear dependent and time dependent behavior of carbon multiwall nanotube suspensions; M.S. Thesis, Chemical & Materials Engineering, University of Kentucky, Lexington, KY, 2001.
161. Wood, J.R.; Zhao, Q.; Wagner, H.D. Orientation of carbon nanotubes in polymers and its detection by Raman spectroscopy. Compos. Part A-Appl. S. **2001**, *32A* (3–4), 391–399.
162. Bower, C.; Rosen, R.; Jin, L.; Han, J.; Zhou, O. Deformation of carbon nanotubes in nanotube-polymer composites. Appl. Phys. Lett. **1999**, *74* (22), 3317–3319.
163. Jin, L.; Bower, C.; Zhou, O.; Alignment of carbon nanotubes in a polymer matrix by mechanical stretching. Appl. Phys. Lett. **1998**, *73* (9), 1197–1199.
164. Bubke, K.; Gnewuch, H.; Hempstead, M.; Hammer, J.; Green, M.L.H. Optical anisotropy of dispersed carbon nanotubes induced by an electric field. Appl. Phys. Lett. **1997**, *71* (14), 1906–1908.
165. Yanagi, H.; Sawada, E.; Manivannan, A.; Nagahara, L.A. Self-orientation of short single-walled carbon nanotubes deposited on graphite. Appl. Phys. Lett. **2001**, *78* (10), 1355–1357.
166. Weisenberger, M. Synthesis and Characterization of Multiwalled Carbon Nanotube/Polyacrylonitrile Composite Fibers and Resulting Carbon Fibers; Chemical & Materials Engineering, University of Kentucky: Lexington, KY, 2002; M. Sc. Thesis.
167. Kim, Y.A.; Hayashi, T.; Fukai, Y.; Endo, M.; Yanagisawa, T.; Dresselhaus, M.S. Effect of ball milling on morphology of cup-stacked carbon nanotubes. Chem. Phys. Lett. **2002**, *355* (3,4), 279–284.
168. Pierard, N.; Fonseca, A.; Konya, Z.; Willems, I.; Van Tendeloo, G.; Nagy, J.B. Production of short carbon nanotubes with open tips by ball milling. Chem. Phys. Lett. **2001**, *335* (1–2), 1–8.
169. Li, Y.B.; Wei, B.Q.; Liang, J.; Yu, Q.; Wu, D.H. Transformation of carbon nanotubes to nanoparticles by ball milling process. Carbon **1999**, *37* (3), 493–497.
170. Niesz, K.; Nagy, J.B.; Fonseca, A.; Willems, I.; Konya, Z.; Vesselenyi, I.; Mehn, D.; Bister, G.; Kiricsi, I. Functional groups generated by mechanical and chemical breaking of multiwall carbon

nanotubes. AIP Conf. Proc. **2001**, *591* (Electronic Properties of Molecular Nanostructures), 345–348.
171. Jia, Z.; Wang, Z.; Liang, J.; Wei, B.; Wu, D. Production of short multi-walled carbon nanotubes. Carbon **1999**, *37* (6), 903–906.
172. Awasthi, K.; Kamalakaran, R.; Singh, A.K.; Srivastava, O.N. Ball-milled carbon and hydrogen storage. Int. J. Hydrogen Energ. **2002**, *27* (4), 425–432.
173. Chen, Y.; Fitz Gerald, J.; Chadderton, L.T.; Chaffron, L. Investigation of nanoporous carbon powders produced by high energy ball milling and formation of carbon nanotubes during subsequent annealing. Mater. Sci. Forum **1999**, *312–314* (Metastable, Mechanically Alloyed and Nanocrystalline Materials), 375–379.
174. Chen, Y.; Fitz Gerald, J.; Williams, J.S.; Bulcock, S. Synthesis of boron nitride nanotubes at low temperatures using reactive ball milling. Chem. Phys. Lett. **1999**, *299* (3,4), 260–264.
175. Chen, Y.; Chadderton, L.T.; Williams, J.S.; Gerald, J.F. Solid-state formation of carbon and boron nitride nanotubes. Mater. Sci. Forum **2000**, *343–346* (Pt. 1, Metastable, Mechanically Alloyed and Nanocrystalline Materials, Part 1), 63–67.
176. Gao, B.; Bower, C.; Lorentzen, J.D.; Fleming, L.; Kleinhammes, A.; Tang, X.P.; McNeil, L.E.; Wu, Y.; Zhou, O. Enhanced saturation lithium composition in ball-milled single-walled carbon nanotubes. Chem. Phys. Lett. **2000**, *327* (1,2), 69–75.
177. Kumar, T.P. Lithium batteries: New materials, developments and perspectives, Edited by G. Pistoia. Bull. Electrochem. **1995**, *11* (3), 167–8.
178. Pistoia, G. Ed. Lithium Batteries: New Materials, Developments and Perspectives. 1994; 482 pp (Ind. Chem. Libr. **1994**, 5).
179. Zhou, O.; Fleming, R.M.; Murphy, D.W.; Chen, C.H.; Haddon, R.C.; Ramirez, A.P.; Glarum, S.H. Defects in carbon nanostructures. Science (Washington, D. C., 1883), **1994**, *263* (5154), 1744–1747.
180. Suzuki, S.; Tomita, M. Observation of potassium-intercalated carbon nanotubes and their valence-band excitation spectra. J. Appl. Phys. **1996**, *79* (7), 3739–3743.
181. Lee, R.S.; Kim, H.J.; Fischer, J.E.; Thess, A.; Smalley, R.E. Conductivity-enhancement in single-walled carbon nanotube bundles doped with K and Br. Nature (London), **1997**, *388* (6639), 255–257.
182. Bower, C.; Suzuki, S.; Tanigaki, K.; Zhou, O. Synthesis and structure of pristine and alkali-metal-intercalated single-walled carbon nanotubes. Appl. Phys. A- Mater. **1998**, *A67* (1), 47–52.
183. Andreoni, W. Ed. *The Physics of Fullerene-Based and Fullerene-Related Materials.*; 2000; 445 pp (Phys. Chem. Mater. Low-Dimens. Struct. **2000**, 23).
184. Slanina, Z. The physics of fullerene-based and fullerene-related materials, Wanda Andreoni, Ed. Fullerene Sci. Technol. **2001**, *9* (4), 561.
185. Chen, J.; Dyer, M.J.; Yu, M.-F. Cyclodextrin-mediated soft cutting of single-walled carbon nanotubes. J. Am. Chem. Soc. **2001**, *123* (25), 6201–6202.
186. Chen, J.; Hamon, M.A.; Hu, H.; Chen, Y.; Rao, A.M.; Eklund, P.C.; Haddon, R.C. Solution properties of single-walled carbon nanotubes. Science **1998**, *282* (5386), 95–98 (Washington, D. C).
187. Chen, J.; Liu, H.; Weimer, W.A.; Halls, M.D.; Waldeck, D.H.; Walker, G.C. Noncovalent engineering of carbon nanotube surfaces by rigid, functional conjugated polymers. J. Am. Chem. Soc. **2002**, *124* (31), 9034–9035.
188. Holzinger, M.; Vostrowsky, O.; Hirsch, A.; Hennrich, F.; Kappes, M.; Weiss, R.; Jellen, F. Sidewall functionalization of carbon nanotubes. Angew. Chem. Int. Edit. **2001**, *40* (21), 4002–4005.
189. Georgakilas, V.; Kordatos, K.; Prato, M.; Guldi, D.M.; Holzinger, M.; Hirsch, A. Organic functionalization of carbon nanotubes. J. Am. Chem. Soc. **2002**, *124* (5), 760–761.
190. Boul, P.J.; Liu, J.; Mickelson, E.T.; Huffman, C.B.; Ericson, L.M.; Chiang, I.W.; Smith, K.A.; Colbert, D.T.; Hauge, R.H.; Margrave, J.L.; Smalley, R.E. Reversible sidewall functionalization of buckytubes. Chem. Phys. Lett. **1999**, *310* (3,4), 367–372.
191. Banerjee, S.; Wong, S.S. Functionalization of carbon nanotubes with a metal-containing molecular complex. Nano Lett. **2002**, *2* (1), 49–53.
192. Varadan, V.K. MEMS- and NEMS-based smart devices and systems. Proceedings of SPIE—The International Society for Optical Engineering, **2001**, *4591*, 28–38 (Electronics and Structures for MEMS II).
193. Tour, J.M.; Bahr, J.L.; Yang, J. Process for derivatizing carbon nanotubes with diazonium species and compositions thereof. PCT Int. Appl. **2002**, 45 pp.
194. Huang, H.; Kajiura, H.; Yamada, A.; Ata, M. Purification and alignment of arc-synthesis single-walled carbon nanotube bundles. Chem. Phys. Lett. **2002**, *356* (5,6), 567–572.
195. Moon, J.-M.; An, K.H.; Lee, Y.H.; Park, Y.S.; Bae, D.J.; Park, G.-S. High-yield purification process of singlewalled carbon nanotubes. J. Phys. Chem. B **2001**,*105* (24), 5677–5681.

196. Esumi, K.; Ishigami, M.; Nakajima, A.; Sawada, K.; Honda, H. Chemical treatment of carbon nanotubes. Carbon **1996**, *34* (2), 279–281.
197. Chen, J.; Rao, A.M.; Lyuksyutov, S.; Itkis, M.E.; Hamon, M.A.; Hu, H.; Cohn, R.W.; Eklund, P.C.; Colbert, D.T.; Smalley, R.E.; Haddon, R.C. Dissolution of full-length single-walled carbon nanotubes. J. Phys. Chem. B **2001**, *105* (13), 2525–2528.
198. Lee, H.-J.; Lee, H. Vertical alignment of chemically modified single-walled carbon nanotubes on self-assembled monolayers containing an amine group. Abstracts of Papers; 223rd ACS National Meeting Orlando, FL, United States, April 7–11, 2002; 2002; COLL-317.
199. Stepanek, I.; De Menorval, L.C.; Edwards, R.; Bernier, P. Carbon nanotubes and gas adsorption. AIP Conf. Proc. **1999**, *486* (Electronic Properties of Novel Materials—Science and Technology of Molecular Nanostructures), 456–461.
200. Colomer, J.F.; Piedigrosso, P.; Mukhopadhyay, K.; Konya, Z.; Willems, I.; Fonseca, A.; Nagy, J.B. Purification of multi-wall carbon nanotubes produced over supported catalysts. Proceedings—Electrochemical Society, 1998; *98-8*, 830–842 (Recent Advances in the Chemistry and Physics of Fullerenes and Related Materials).
201. Nagasawa, S.; Yudasaka, M.; Hirahara, K.; Ichihashi, T.; Iijima, S. Effect of oxidation on single-wall carbon nanotubes. Chem. Phys. Lett. **2000**, *328* (4,5,6), 374–380.
202. Bahr, J.L.; Yang, J.; Kosynkin, D.V.; Bronikowski, M.J.; Smalley, R.E.; Tour, J.M. Functionalization of carbon nanotubes by electrochemical reduction of aryl diazonium salts: A bucky paper electrode. J Am. Chem. Soc. **2001**, *123* (27), 6536–6542.
203. Mawhinney, D.B.; Naumenko, V.; Kuznetsova, A.; Yates, J.T., Jr.; Liu, J.; Smalley, R.E. Infrared spectral evidence for the etching of carbon nanotubes: Ozone oxidation at 298 K. J. Am. Chem. Soc. **2000**, *122* (10), 2383–2384.
204. Satishkumar, B.C.; Govindaraj, A.; Mofokeng, J.; Subbanna, G.N.; Rao, C.N.R. Novel experiments with carbon nanotubes: Opening, filling, closing and functionalizing nanotubes. J. Phys. B-At. Mol. Opt. **1996**, *29* (21), 4925–4934.
205. Jeong, T.; Kim, W.-Y.; Hahn, Y.-B. A new purification method of single-wall carbon nanotubes using H2S and O2 mixture gas. Chem. Phys. Lett. **2001**, *344* (1,2), 18–22.
206. Jeong, T.; Kim, T.H.; Kim, W.-Y.; Lee, K.-H.; Hahn, Y.-B. High yield purification of carbon nanotubes with H2S-O2 mixture. Korean J. Chem. Eng. **2002**, *19* (3), 519–523.
207. Ago, H.; Kugler, T.; Cacialli, F.; Salaneck, W.R.; Shaffer, M.S.P.; Windle, A.H.; Friend, R.H. Work functions and surface functional groups of multiwall carbon nanotubes. J. Phys. Chem. B **1999**, *103* (38), 8116–8121.
208. Kuznetsova, A.; Popova, I.; Yates, J.T., Jr.; Bronikowski, M.J.; Huffman, C.B.; Liu, J.; Smalley, R.E.; Hwu, H.H.; Chen, J.G. Oxygen-containing functional groups on single-wall carbon nanotubes: NEXAFS and vibrational spectroscopic studies. J. Am. Chem. Soc. **2001**, *123* (43), 10699–10704.
209. Satishkumar, B.C.; Vogl, E.M.; Govindaraj, A.; Rao, C.N.R. The decoration of carbon nanotubes by metal nanoparticles. J. Phys. D Appl. Phys. **1996**, *29* (12), 3173–3176.
210. Yu, R.; Chen, L.; Liu, Q.; Lin, J.; Tan, K.-L.; Ng, S.C.; Chan, H.S.O.; Xu, G.-Q.; Hor, T.S.A. Platinum deposition on carbon nanotubes via chemical modification. Chem. Mater. **1998**, *10* (3), 718–722.
211. Bond, A.M.; Miao, W.; Raston, C.L. Mercury(II) immobilized on carbon nanotubes: synthesis, characterization, and redox properties. Langmuir **2000**, *16* (14), 6004–6012.
212. Lee, C.-J.; Yoo, J.-E. Acidic gas phase for purification of carbon nanotubes by heat treatment in a tube furnace. Eur. Pat. Appl. **2000**, 8.
213. Martinez, M.T.; Callejas, M.A.; Benito, A.M.; Maser, W.K.; Cochet, M.; Andres, J.M.; Schreiber, J.; Chauvet, O.; Fierro, J.L.G. Microwave single walled carbon nanotubes purification. Chem. Commun. (Camb) FIELD Publication Date:2002 May 7 (9), 1000–1. FIELD Reference Number: FIELD Journal Code: 9610838 FIELD Call Number.
214. Kyotani, T.; Nakazaki, S.; Xu, W.-H.; Tomita, A. Chemical modification of the inner walls of carbon nanotubes by HNO3 oxidation. Carbon **2001**, *39* (5), 782–785.
215. Zhu, H.W.; Chen, A.; Mao, Z.Q.; Xu, C.L.; Xiao, X.; Wei, B.Q.; Liang, J.; Wu, D.H. The effect of surface treatments on hydrogen storage of carbon nanotubes. J. Mater. Sci. Lett. **2000**, *19* (14), 1237–1239.
216. Eswaramoorthy, M.; Sen, R.; Rao, C.N.R. A study of micropores in single-walled carbon nanotubes by the adsorption of gases and vapors. Chem. Phys. Lett. **1999**, *304* (3,4), 207–210.
217. Margrave, J.L.; Mickelson, E.T.; Hauge, R.; Boul, P.; Huffman, C.B.; Liu, J.; Smalley, R.E.; Smith, K.; Colbert, D.T. Chemical derivatization of

single-wall carbon nanotubes to facilitate solvation for carbon fiber synthesis. PCT Int. Appl. **2000**, 76.
218. Margrave, J.L.; Mickelson, E.T.; Chiang, I.W.; Zimmerman, J.L.; Boul, P.J.; Lozano, J.; Liu, J.; Smalley, R.E.; Hauge, R.H. Solvation of fluorinated single-wall carbon nanotubes in alcohol solvents. *Book of Abstracts*, 218th ACS National Meeting, New Orleans, Aug. 22–26, 1999; FLUO-013.
219. Chiang, I.W.; Michelson, E.T.; Boul, P.J.; Hauge, R.H.; Smalley, R.E.; Margrave, J.L. Fluorination, defluorination, and derivatization of single-wall carbon nanotubes. Abstr. Pap.–Am. Chem. Soc. **2000**, *220th*, IEC-153.
220. Mukhopadhyay, I.; Yokoyama, Y.; Okino, F.; Kawasaki, S.; Touhara, H.; Hsu, W.K. Effect of chemical modification on electrochemical Li insertion in highly ordered multi-wall carbon nanotubes. Proceedings–Electrochemical Society **2001**; *2001–2014* (Reactive Intermediates in Organic and Biological Electrochemistry), 37–40.
221. Seifert, G.; Kohler, T.; Frauenheim, T. Molecular wires, solenoids, and capacitors by sidewall functionalization of carbon nanotubes. Appl. Phys. Lett. **2000**, *77* (9), 1313–1315.
222. Gu, Z.; Peng, H.; Zimmerman, J.L.; Chiang, I.W.; Khabashesku, V.N.; Hauge, R.H.; Margrave, J.L. Fluorination of polymeric C60 and carbon nanotubes: A starting point for various chemical modifications of nanostructured carbon materials. *Abstracts of Papers*, 223rd ACS National Meeting, Orlando, FL, United States, April 7–11, 2002; 2002; FLUO-012.
223. Kooi, S.E.; Schlecht, U.; Burghard, M.; Kern, K. Electrochemical modification of single carbon nanotubes. Angew Chem. Int. Edit. **2002**, *41* (8), 1353–1355.
224. Pekker, S.; Salvetat, J.P.; Jakab, E.; Bonnard, J.M.; Forro, L. Chemical functionalization of carbon nanotubes. AIP Conf. Proc. **1999**, *486* (Electronic Properties of Novel Materials—Science and Technology of Molecular Nanostructures), 474–477.
225. Wang, X.; Liu, Y.; Qiu, W.; Zhu, D. Immobilization of tetra-tert-butylphthalocyanines on carbon nanotubes: A first step towards the development of new nanomaterials. J. Mater. Chem. **2002**, *12* (6), 1636–1639.
226. Shim, M.; Kam, N.W.S.; Chen, R.J.; Li, Y.; Dai, H. Functionalization of carbon nanotubes for biocompatibility and biomolecular recognition. Nano Lett. **2002**, *2* (4), 285–288.
227. Chen, Q.; Dai, L.; Gao, M.; Huang, S.; Mau, A. Plasma activation of carbon nanotubes for chemical modification. J. Phys. Chem. B **2001**, *105* (3), 618–622.
228. Hunter, R.J. *Foundations of Colloid Science*; Oxford University Press: New York, 1986; Vol. 1, 600 pp.
229. Riggs, J.E.; Walker, D.B.; Carroll, D.L.; Sun, Y.-P. Carbon nanotubes as optical limiters. Proceedings–Electrochemical Society, 2000; 2000-10 (Fullerenes 2000—Volume 8: Electrochemistry and Photochemistry), 267–280.
230. Hwang, K.C. Synthesis of SO2-carbon nanotubes-micro rods and their applications in reinforcements of ceramics. Abstr. Pap.—Am. Chem. Soc. **2000**, *220th*, PHYS-387.
231. Sun, Y.-P.; Riggs, J.E.; Martin, B.; Carroll, D.L. Optical limiting properties of suspended and solubilized carbon nanotubes. Abstr. Pap.—Am. Chem. Soc. **2000**, *220th*, IEC-152.
232. Duesberg, G.S.; Muster, J.; Krstic, V.; Burghard, M.; Roth, S. Chromatographic size separation of single-wall carbon nanotubes. Appl. Phys. A-Mater. **1998**, *A67* (1), 117–119.
233. Duesberg, G.S.; Burghard, M.; Muster, J.; Philipp, G.; Roth, S. Separation of carbon nanotubes by size exclusion chromatography. Chem. Commun. (Cambridge) **1998**, (3), 435–436.
234. Vigolo, B.; Penicaud, A.; Coulon, C.; Sauder, C.; Pailler, R.; Journet, C.; Bernier, P.; Poulin, P. Dispersions and fibers of carbon nanotubes. Materials Research Society Symposium Proceedings **2001**, *633* (Nanotubes and Related Materials), A12.1.1–A12.1.9.
235. Liu, J.; Rinzler, A.G.; Dai, H.; Hafner, J.H.; Bradley, R.K.; Boul, P.J.; Lu, A.; Iverson, T.; Shelimov, K.; Huffman, C.B.; Rodriguez-Macias, F.; Shon, Y.-S.; Lee, T.R.; Colbert, D.T.; Smalley, R.E. Fullerene pipes. Science (Washington, D. C.) **1998**, *280* (5367), 1253–1256.
236. Lewenstein, J.C.; Burgin, T.P.; Ribayrol, A.; Nagahara, L.A.; Tsui, R.K. High-yield selective placement of carbon nanotubes on pre-patterned electrodes. Nano Lett. **2002**, *2* (5), 443–446.
237. Burghard, M.; Duesberg, G.; Philipp, G.; Muster, J.; Roth, S. Controlled adsorption of carbon nanotubes on chemically modified electrode arrays. Adv. Mater. (Weinheim, Germany) **1998**, *10* (8), 584–588.
238. Riggs, J.E.; Walker, D.B.; Carroll, D.L.; Sun, Y.-P. Optical limiting properties of suspended and solubilized carbon nanotubes. J. Phys. Chem. B **2000**, *104* (30), 7071–7076.
239. Krstic, V.; Muster, J.; Duesberg, G.S.; Philipp, G.; Burghard, M.; Roth, S. Electrical transport in single-walled carbon nanotube bundles embedded in Langmuir-Blodgett monolayers. Synthetic Met. **2000**, *110* (3), 245–249.

240. Krstic, V.; Duesberg, G.S.; Muster, J.; Burghard, M.; Roth, S. Langmuir-Blodgett films of matrix-diluted single-walled carbon nanotubes. Chem. Mater. **1998**, *10* (9), 2338–2340.
241. Bandyopadhyaya, R.; Nativ-Roth, E.; Regev, O.; Yerushalmi-Rozen, R. Stabilization of individual carbon nanotubes in aqueous solutions. Nano Lett. **2002**, *2* (1), 25–28.
242. Ma, C.; Xia, Y. Mixed adsorption of sodium dodecyl sulfate and ethoxylated nonylphenols on carbon black and the stability of carbon black dispersions in mixed solutions of sodium dodecyl sulfate and ethoxylated nonylphenols. Colloids Surf. **1992**, *66* (3), 215–221.
243. Asakawa, T.; Kaneko, Y.; Ogino, K. Removal of trace amounts of multicomponent organic compounds dissolved in water. II. Adsorption on carbon adsorbents for phenol and anionic surfactant mixtures. I. Yukagaku **1986**, *35* (5), 367–372.
244. Vaeck, S.V.; Merken, G.V. Some experiments on detergency in aqueous and nonaqueous media. XII. Further studies on the interactions between surfactants, electrolytes and pH in the deposition of hydrophobic particulate soil. Tenside Deterg. **1981**, *18* (3), 126–129.
245. Sandstrom, P.H. Free-flowing SBR black masterbatch powder. U.S. **1983**, 7.
246. Gonzalez-Garcia, C.M.; Gonzalez-Martin, M.L.; Gomez-Serrano, V.; Bruque, J.M.; Labajos-Broncano, L. Determination of the free energy of adsorption on carbon blacks of a nonionic surfactant from aqueous solutions. Langmuir **2000**, *16* (8), 3950–3956.
247. Garamus, V.M.; Pedersen, J.S. A small-angle neutron scattering study of the structure of graphitized carbon black aggregates in Triton X-100/water solutions. Colloid. Surface. A **1998**, *132* (2–3), 203–212.
248. Zhao, Z.; Gu, T. Adsorption and wetting. II. Adsorption of Triton X-100 and Triton-305 onto carbon black from water and cyclohexane solutions. Huaxue Xuebao **1987**, *45* (7), 645–650.
249. Nagahara, L.; Burgin, T.; Lewenstein, J.; Harvey, T., III; Shieh, C.-L.; Tsui, R. Surfactant removal from carbon nanotubes. IP.com Journal **2001**, *1* (5), 65.
250. Peigney, A.; Laurent, C.; Flahaut, E.; Rousset, A. Carbon nanotubes as a part of novel ceramic matrix nanocomposites. Advances in Science and Technology (Faenza, Italy), **1999**, *15* (Ceramics: Getting into the 2000's, Pt. C), 593–604.
251. Peigney, A.; Laurent, C.; Flahaut, E.; Rousset, A. Carbon nanotubes in novel ceramic matrix nanocomposites. Ceramics International **2000**, *26* (6), 677–683.
252. Peigney, A.; Laurent, C.; Rousset, A. Synthesis and characterization of alumina matrix nanocomposites containing carbon nanotubes. Key Eng. Mat. **1997**, *132–136* (Pt. 2, Euro Ceramics V), 743–746.
253. Hwang, G.L.; Hwang, K.C. Carbon nanotube reinforced ceramics. J. Mater. Chem. **2001**, *11* (6), 1722–1725.
254. Hwang, G.L.; Hwang, K.C. Breakage, fusion, and healing of carbon nanotubes. Nano Lett. **2001**, *1* (8), 435–438.

Received October 10, 2002
Accepted October 16, 2002